Insights into Crustal Assimilation by Icelandic Basalts from Boron Isotopes in Melt Inclusions from the 1783-1784 Lakagígar Eruption

Maryjo Brounce[1†], Maureen Feineman[1*], Peter LaFemina[1] and Andrey Gurenko[2‡]

[1]The Pennsylvania State University, Department of Geosciences, University Park, PA, 16802, USA

[2]Woods Hole Oceanographic Institute, Department of Geology and Geophysics, Woods Hole, MA, 02543, USA

[†] Now at University of Rhode Island, Graduate School of Oceanography, Department of Marine Geology and Geophysics, Narragansett, RI, 02882, USA

[‡]Now at Centre de Recherches Pétrographiques et Géochimiques, CNRS-Nancy Université, BP 20, F-54501 Vandoeuvre-lès-Nancy, France

* Corresponding author

ABSTRACT

The boron isotope system has great potential for tracing alteration and assimilation in basaltic systems due to the very low concentrations of B in mantle-derived melts and the strong isotopic contrast between the mantle and surface materials. However, variability in B concentrations and isotope ratios in basalts can also be interpreted to reflect inputs from enriched regions of the mantle, as the extent of mantle heterogeneity with respect to boron remains poorly delineated. We have determined boron concentrations and isotope ratios in fresh, glassy, plagioclase-hosted melt inclusions and unaltered scoriaceous matrix glasses from four localities associated with the 1783-1784 Lakagígar (Laki Fissure) eruption, Iceland. Boron concentrations range from 0.59-1.25 ppm in the melt inclusions, and from 1.25-1.65 ppm in the matrix glasses, while $\delta^{11}B_{NBS-951}$ ranges from -7.8‰ to -16.5‰ in the melt inclusions and -10.5‰ to -16.9‰ in the matrix glasses. In contrast to previous studies of boron in basaltic melt inclusions from other fissure swarms in Iceland (Gurenko and Chaussidon, 1997, *Chem. Geol.* 135, 21-34), the Lakagígar melt inclusions display a significant range of boron concentrations and isotope ratios at constant K_2O wt.%, which is more consistent with B addition by assimilation of altered basalt than it is with mixing between depleted and enriched mantle sources. Assimilation of freshwater-altered crustal materials at depth may impart a light $\delta^{11}B$ signature such as that observed in the Lakagígar melt inclusions and tephra host glasses. Considering boron concentrations and isotope ratios in the Lakagígar glasses and previously studied altered Icelandic basalts, together with volatile equilibration depths of the Lakagígar melt inclusions, we propose that a) mantle-derived magmas formed beneath Lakagígar assimilated ~5-20% altered crust at a depth of ~3-4 km or more, probably during magma accumulation in sills formed at the boundaries of low-density hyaloclastite layers; and b)

the magma subsequently underwent extensive mixing and homogenization prior to eruption, quite possibly within the magma chamber beneath the Grímsvötn central volcano, assimilating an additional ~10% of altered crust at that time, for a total of up to 30% crustal assimilation. We hypothesize that volatiles including H_2O, CO_2, S, F, and Cl, which were responsible for the majority of the considerable casualties attributed to the Lakagígar eruption, were added together with isotopically light B by assimilation of hydrothermally altered crustal materials.

1. INTRODUCTION AND GEOLOGICAL BACKGROUND

Explosive, large volume eruptions impact climate and environment at local, regional and global scales. The Mid-Atlantic Ridge is expressed in Iceland in the form of sub-aerial neovolcanic zones (Figure 1a). Magmatic systems in these neovolcanic zones consist of central volcanoes with crustal magma chambers and fissure swarms that accommodate plate spreading via lateral magma injection (Sigurdsson and Sparks, 1976). Holocene basaltic fissure eruptions in Iceland are among the largest historic eruptions on Earth and have had profound global impacts (Thorarinsson, 1979). The 1783-84 Lakagígar eruption (also known as Laki Fissure, or the "Skaftár Fires") was one of the most voluminous single eruptions of historic times. The fissure starts 50 kilometers southwest of the Grímsvötn central volcano and presumably continues beneath Vatnajökull to intersect with Grímsvötn itself, bisecting the older Laki hyaloclastite mountain (Figure 1b). Starting in June 1783 and continuing into January 1784, the fissure first erupted to the southwest near the Skaftá River and proceeded to the northeast back toward Grímsvötn,

producing ~14.7 km^3 of lava, ~0.4 km^3 of tephra and ~10^{12} tons of volatiles, including ~10^{11} tons each of sulfur aerosols, H_2O, and CO_2, and smaller but significant amounts of HF and HCl (Thorarinsson, 1979; Thordarson and Self, 1993; Thordarson et al.,1996). Famine, disease, and the harsh winter following the eruption are all attributed to the tephra and, more importantly, the aerosols released. All told, these factors claimed as many as 10,000 lives worldwide, making the 1783-84 Lakagígar eruption not only one of the most voluminous, but also one of the deadliest historic eruptions (Thorarinsson, 1979; Tilling, 1996).

The striking geochemical homogeneity of the large volume of lava erupted from Lakagígar (Sigmarsson and Condomines, 1991) suggests efficient mixing in a large magma chamber at some level beneath the surface. If magma accumulation does occur at one or more levels in the crust, then we might expect to find some record of crustal assimilation. Indeed, previous geochemical studies indicate variable amounts of crustal assimilation prior to eruption at Lakagígar. Sigmarsson and Condomines (1991) infer assimilation of metabasalts on the order of ~20%, accompanied by magma mixing at the crust-mantle boundary, based on U and Th concentrations and Sr, Th and O isotope ratios. Others suggest shallower assimilation of up to 60% hydrothermally altered crustal materials based on isotopic data from basalts and melt inclusions, as well as phenocryst-matrix oxygen isotopic disequilibrium in Lakagígar lavas (Hattori and Muehlenbachs, 1982; Hémond et al., 1988; Bindeman et al., 2006, 2008). Métrich et al. (1991) suggest a shallow level for magma mixing (~4 km), perhaps within the Grímsvötn magma chamber, based on compositional trends and volatile concentrations observed in melt

inclusions, while Bindeman et al. (2006, 2008) argue for extensive assimilation at depths below the central magma chamber. Note that these interpretations are by no means mutually exclusive.

Boron isotope ratios ($^{11}B/^{10}B$, expressed as $\delta^{11}B = (((^{11}B/^{10}B)_{unknown}/(^{11}B/^{10}B)_{standard} - 1)*1000$ in permil variation relative to the NBS-951 boric acid standard) have the potential to contribute uniquely to understanding crustal assimilation at basaltic fissures. Boron isotopes are not strongly fractionated during crystallization of magma (Benton et al., 1999), and boron is compatible in basaltic melt relative to fluid at low pressures, such that boron loss during degassing of basalts is likely to be limited (Hervig et al., 2002). Since boron is present in low concentrations in primitive basaltic magmas (~0.5-1.0 ppm, Chaussidon and Marty, 1995), $\delta^{11}B$ is very sensitive to alteration and assimilation of altered crustal materials. In addition to crustal inputs, however, we must consider the boron concentrations and isotope ratios in the parental magma, which is not at all straightforward.

Previous analyses of basaltic melt inclusions and tephra host glasses suggest that the mantle source region for Icelandic basalts is uniformly light with respect to $\delta^{11}B$ (-11.3, $2\sigma \pm 3.8‰$; Gurenko and Chaussidon, 1997). In glasses from the Reykjanes and Hengill fissure swarms (Figure 1a), B concentrations increase with increasing K_2O wt.%. It has been demonstrated that B and K are not strongly fractionated by mantle melting (Ryan and Langmuir, 1993), such that variations in melt fraction will cause B and K_2O concentrations in a suite of basalts to co-vary with a constant B/K_2O as long as they are

106 derived from a homogeneous mantle source. The Reykjanes melt inclusions, which are
107 sampled at an area relatively far from the center of the presumed Icelandic plume (where
108 the plume center is at a location approximately equivalent to the 40 km Moho contour
109 shown in Figure 1a), are characterized by mid-ocean ridge (MORB)-like values, with
110 average $B/K_2O = 20$ at K_2O <0.1%. The Hengill melt inclusions, which are sampled
111 from an area somewhat closer to the Icelandic plume, range from MORB-like values
112 similar to those at Reykjanes to more ocean island basalt (OIB)-like values at K_2O = 0.1-
113 0.4 wt.%. The more enriched melt inclusions from Hengill are characterized by a
114 relatively constant B/K_2O = ~4, consistent with B addition from a plume-related source.
115 Lakagígar, which lies still closer to the center of the presumed Icelandic plume (Figure
116 1a), should by the same logic extend to higher B and K_2O concentrations at roughly the
117 same B/K_2O, with similarly invariant light $\delta^{11}B$.
118
119 The purpose of this study is to determine to what extent the boron concentrations and
120 isotope ratios at Lakagígar are controlled by the mantle source, which in this case would
121 include an enriched OIB-like contribution characterized by unusually light $\delta^{11}B$, and to
122 what extent they are controlled by assimilation of altered crustal materials. To this end,
123 we present new boron concentration and isotope ratio data, as well as lithium
124 concentrations, volatile concentrations, and major element compositions of tephra matrix
125 glasses and plagioclase-hosted melt inclusions from the 1783-1784 Lakagígar eruption.
126 Modeling of these data help constrain the source of the parent magma and the magnitude
127 of crustal assimilation, and provide a tentative clue to the source of the volatiles that were
128 so destructive in the aftermath of this eruption.

2. METHODS

2.1 Sample Selection

We sampled four tephra units originating (presumably) from two tuff cones, representative of the phreatomagmatic stages of the 1783-84 eruption (Figure 1b). Loose plagioclase phenocrysts were hand-picked from the tephras under a binocular microscope. In some cases, melt inclusions were clearly visible within the transparent crystals. The plagioclase crystals were mounted in epoxy and polished to expose the melt inclusions at the surface (Figure 2a). Melt inclusions were chosen for analysis based on the following criteria: 1) lack of visible daughter crystals; 2) clean, sharp contacts with the host crystal; 3) lack of any cracks or breaches from the melt inclusion to the crystal surface. In addition to melt inclusions, several intact scoria lapilli from each tephra sample were mounted in epoxy and polished for analysis of the matrix glass. The scoria samples studied were selected to be free of secondary alteration products. Microlites of plagioclase were ubiquitous in the matrix glasses (Figure 2b), and spots for analysis were carefully chosen to avoid these crystals.

2.2 Major Elements

Major element compositions were obtained using a Cameca SX-50 Electron Probe Micro-Analyzer (EPMA) at Penn State. The instrument was operated at an accelerating voltage of 15 keV and a beam current of 12 nA. Glasses were analyzed using a defocused electron beam (~20μm) to minimize Na volatilization, while plagioclase phenocrysts were analyzed using a focused electron beam (~1μm). The x-ray intensity

data were subject to a PAP (phi-rho-z) matrix correction algorithm as described in Pouchou and Pichoir (1987), and converted to concentrations by comparison to natural and synthetic standards. All samples were carbon-coated prior to EPMA analysis.

2.3 Boron and Lithium Concentrations and Boron Isotope Ratios

Boron and lithium concentrations and boron isotope ratios were analyzed in the scoria and plagioclase-hosted melt inclusions by Secondary Ionization Mass Spectrometry (SIMS) using the Cameca IMS 3f (some Li and B concentrations) or Cameca IMS 1280 (most concentrations and all isotope ratios) at the Northeast National Ion Microprobe Facility at the Woods Hole Oceanographic Institute (WHOI), following the techniques described by Chaussidon and Jambon (1994) and Chaussidon et al. (1997).

2.3.1 Cameca IMS 3f

Standards and unknown samples were sputtered with a nominal 8.3 kV $^{16}O^-$ primary beam focused to about 20−30 μm in diameter. Instrument conditions are provided in Supplemental Data (Table S1). Each analysis consisted of 5 sequential blocks of the masses ^{7}Li, ^{11}B and ^{30}Si. Element concentrations relative to independently known SiO_2 concentrations were calculated using calibration curves obtained by linear regressions of a set of 3 reference glasses (NBS-610, 357 ppm B; NBS-612, 35 ppm B; and KL-2G, 3 ppm B; values from Jochum et al., 2000 and Rosner et al., 2008; calibration line shown in Supplemental Data, Figure S1a). Instrument drift was monitored and corrected using daily replicate analyses of KL2-G reference glass. The analytical precision was better than 15% relative standard deviation.

175

176 *2.3.2 Cameca IMS 1280*

177 Standards and unknown samples were sputtered with a nominal 13 kV $^{16}O^-$ primary beam
178 focused to approximately 20-25 μm in diameter. Instrument settings are given in
179 Supplemental Data Table S1. Samples were sputtered for 500 seconds before they were
180 analyzed, and each measurement included 50 cycles for element concentrations or 200-
181 250 cycles for boron isotope ratios. Boron and lithium concentrations were calculated
182 relative to independently known SiO_2 concentrations in the unknown samples of interest
183 using calibration lines obtained by linear regression of measurements made on a set of
184 five reference glasses (GOR128-G, 20 ppm B; StHs6/80-G, 11.6 ppm B; ATHO-G, 6
185 ppm B; KL-2G, 3 ppm B; and ML3B-G, 2 ppm B; values from Jochum et al., 2000 and
186 Rosner et al., 2008), as shown in Supplemental Data, Figure S1b. Analytical precision
187 was ~5-10% relative standard deviation for boron and less than 5% relative standard
188 deviation for lithium.

189

190 For isotope ratio measurements, the instrumental fractionation factor was determined
191 based on multiple measurements of the MPI-DING glass standard StHs6/80-G (11.6 ppm
192 B, $\delta^{11}B = -4.39‰$; Rosner et al., 2008). The suitability of this standard was verified by
193 analyzing its boron isotope ratios in the same session with five other standard reference
194 glasses (NBS-610, NBS-612, Rosner et al., 2008; GOR-128G, GOR-132G, GB4-CRPG,
195 Rosner and Meixner, 2004). The isotope ratio data for the six standards are linearly
196 correlated when plotted against the known $\delta^{11}B$ values, with $r^2 = 0.982$ and $\alpha = 0.9714$
197 for this session (Supplemental Data, Figure S1c). The stability of the instrument and

198 relative homogeneity of the glass standard were verified by comparing repeat analyses of
199 StHs6/80-G over the course of the 3-day session, which yields an average $^{11}B/^{10}B$ of
200 3.9315 ± 0.0111 (2σ external; Figure S1d). Reported uncertainties on unknowns (Table
201 1) are 2σ internal precision on individual measurements, which are greater than the
202 external reproducibility of the standard. All isotope ratios are expressed as $\delta^{11}B$
203 calculated relative to the NBS-951 standard ($^{11}B/^{10}B = 4.04558 \pm 0.00033$; Spivack and
204 Edmond, 1986).
205
206 **2.4 Volatile Concentrations**
207 Concentrations of the volatile species CO_2, H_2O, F, S, and Cl were determined using the
208 Cameca IMS 1280 at WHOI, following the methods described by Hauri et al. (2002) and
209 Shimizu et al. (2009). The samples were carefully polished to remove residual carbon
210 from the carbon-coating process used in preparation for prior analysis by EPMA, then
211 removed from the epoxy mount, cleaned, and remounted by pressing them into indium
212 metal. Samples were sputtered with a 10 kV Cs^+ primary beam focused to 10-20 μm
213 diameter. Instrument settings are given in Supplemental Data Table S1. The
214 measurements were started after a 200 second pre-sputtering, and some spots required
215 multiple analytical cycles to remove unnaturally high concentrations of residual carbon
216 from the carbon coating. Six reference glasses (GL07 51-3, ALV519-4-1, EN113 46D,
217 ALV1649-3, ALV1654-3, FRND 6001; volatile concentration values as in Helo et al.,
218 2011) were analyzed to create the calibration lines used to calculate absolute
219 concentrations of volatile species in the unknown samples (Supplemental Data Figure
220 S2).

221

222 **3. RESULTS**

223 Major element concentrations, boron and lithium concentrations, boron isotope ratios,
224 and volatile data are presented in Table 1, and selected data are presented in Figures 3
225 and 4.

226

227 **3.1 Analytical Results**

228 Although the Lakagígar glasses measured here are, overall, homogeneous tholeiitic
229 basalts (SiO_2 wt % ~48.5-50.5), subtle variations can be observed in the major and
230 incompatible element data. For example, the melt inclusions have higher Mg numbers
231 [Mg# = molar Mg/(Mg+Fe)x100], ranging from ~43-46 with an outlier at 51, relative to
232 the scoria host glasses, which have Mg numbers ~39-41 (Figure 3a and b). We observe a
233 moderately wide range of TiO_2 (~1.8-3.1 wt.%) over a very restricted range of Mg# in the
234 melt inclusions, which is not consistent with fractional crystallization from a common
235 parent magma. In contrast, correlation between TiO_2 and Mg# in the *host glasses* could
236 reflect a small amount of crystallization, likely occurring upon eruption. The rather good
237 correlation between CaO/Al_2O_3 and Mg# over the complete range of glasses analyzed
238 (Figure 3b) is consistent with fractional crystallization of clinopyroxene, although the
239 trend is not observed *within* the suite of melt inclusions with Mg# = 43-46.
240 Clinopyroxene is believed to be a late-crystallizing phase in the Lakagígar basalts (Bell
241 and Humphries, 1972). The matrix glasses have extremely restricted ranges of TiO_2 and
242 total alkalis (Na_2O+K_2O) relative to the melt inclusions (Figure 3c), with the matrix
243 glasses occupying the extreme high end of the range observed in TiO_2 wt % of the

244 inclusions. The matrix glasses and melt inclusions overlap in terms of B concentrations,
245 with the matrix glasses extending toward higher B concentrations and the melt inclusions
246 extending toward lower B concentrations (Figure 3d). While the major and minor
247 element correlations in the Lakagígar glasses are generally weak and characterized by
248 exceptions, the Li vs. B and $\delta^{11}B$ vs. B trends are relatively clear, and more or less
249 continuous from the inclusions to the hosts glasses (Figures 3e and f).
250
251 A few characteristic melt inclusion types can be identified from among the larger dataset.
252 Most notably, inclusion 17pl3a is characterized by significantly higher Mg# (51) and
253 CaO wt % (10.82) relative to all the other inclusions analyzed in this study (43-46 and
254 9.41-9.76, respectively). In contrast, inclusion 17pl3b, which is located in the same
255 phenocryst (slightly closer to the edge), has a lower Mg# (43) more typical of the
256 Lakagígar melt inclusions, and high TiO_2 wt . % (2.98) that overlaps with that of the host
257 glasses. Inclusions 12pl1a and c, both trapped in the same melt inclusion, are outliers in
258 terms of their high total alkali contents (Na_2O+K_2O wt.% = 3.6-3.8), low B and Li
259 concentrations (0.59 and 3.31 ppm, respectively), and relatively high $\delta^{11}B$ (-7.8‰).
260 Inclusion 8pl3a has the highest boron concentration (1.25 ppm) and lightest $\delta^{11}B$ (-
261 16.5‰) of any melt inclusion analyzed, but is in no way distinguishable from the
262 "typical" Lakagígar melt inclusions in terms of major and incompatible element
263 characteristics. Inclusion 14pl1a is most similar to the matrix glasses in terms of TiO_2
264 and total alkalis, and has relatively light $\delta^{11}B$ (-13.9‰). Relative to the melt inclusions,
265 the host glasses are more homogeneous, and are characterized by relatively high TiO_2,
266 low Mg#, high boron and lithium concentrations, and light $\delta^{11}B$.

The volatile components (H_2O, CO_2, S, F, Cl) display a broadly positive correlation with B concentrations in the melt inclusions (Figure 4a-e). The host glasses, in contrast, have slightly higher B concentrations despite being strongly degassed with respect to H_2O, CO_2, and S (Figure 4a, b, and c). The halogens F and Cl are only partially degassed in the matrix glasses relative to the melt inclusions, and in fact some melt inclusions have lower F and Cl concentrations than the host glasses (Figure 4d and e). Despite the fact that both H_2O and CO_2 seemingly correlate with boron concentrations, the correlation between H_2O and CO_2 in the melt inclusions is somewhat ambiguous (Figure 4f), and will be discussed in more detail in Section 4.

3.2 Effects of Post-Entrapment Crystallization

Attempts to correct the melt inclusion compositions for post-entrapment crystallization of plagioclase using both the method of Kress and Ghiorso (2004) and that of Hamada and Fujii (2007) predicted unreasonably large degrees of post-entrapment crystallization (on the order of 25-60%). The method of Kress and Ghiorso (2004), which uses the MELTS software package, does not adequately account for the affect of H_2O in the magma, which serves to increase the anorthite content of plagioclase in equilibrium with a given melt composition. The method of Hamada and Fujii (2007), which utilizes an empirically determined pressure-, temperature-, and composition- dependent partition coefficient, predicted unreasonably high degrees of crystallization for melt inclusions from Izu-Oshima with H_2O contents 0.2-1.4%, comparable to the Lakagígar melt inclusions. Hamada and Fujii (2007) attribute this mismatch to hydrogen loss by diffusion, which

caused them to under-estimate the H_2O contents of the melt inclusions at the time of the final stage of post-entrapment crystallization. As will be discussed in Section 4.5, under-estimation of the initial H_2O contents is possible for the Lakagígar melt inclusions as well. It is also possible that the composition-dependent partition coefficient of Hamada and Fujii (2007) still does not adequately describe the effect of H_2O in the melt on the anorthite content of equilibrium plagioclase.

The boron and volatile concentrations in the melt inclusions presented here have not been corrected for post-entrapment crystallization. Careful visual inspection by transmitted light, reflected light, backscattered and secondary electron imaging suggests a lack of significant post-entrapment crystallization; however, visual detection of post-entrapment crystallization is not always possible. Boron is incompatible during crystallization of An-rich plagioclase from basalt (Bindeman et al., 1998). Métrich et al. (1991) calculated 2-11% post-entrapment crystallization of Lakagígar melt inclusions, mostly based on olivine-hosted inclusions. Thus we estimate that a limited amount of post-entrapment crystallization may have increased B and volatile concentrations in the melt inclusions by up to 10% relative to their values at the time of entrapment, which is within the uncertainty of the data. Boron isotopes are not fractionated by crystallization of basaltic magma (Benton et al., 1999), so no correction is needed.

4. DISCUSSION

4.1 Compositional Variation in Lakagígar Glasses

4.1.1 Major elements

313 Although the melt inclusions from Lakagígar are relatively homogeneous in terms of
314 their major element compositions (SiO_2 = 48.4-50.6 wt.%; Na_2O+K_2O = 2.70-3.73; Mg#
315 = 43-46, with one inclusion at 51), several compositional outliers can be identified. For
316 example, inclusions 12pl1a and 12pl1c have high total alkalis, while 14pl1a and 17pl3b
317 have high TiO_2, and 17pl3a has distinctively high Mg# and CaO, coupled with low TiO_2
318 (Figure 3). We interpret, based on the compositional contrast between inclusions 17pl3a
319 and 17pl3b (hosted in the same phenocryst, but slightly closer to the rim), that inclusion
320 17pl3a is most likely trapped in a xenocrystic plagioclase core that was later overgrown
321 by new plagioclase. The xenocrystic core represents either an earlier incarnation of the
322 Lakagígar-Grímsvötn magmatic system or even another magmatic system entirely; such
323 xenocrysts have been previously recognized in Lakagigar magmas on the basis of oxygen
324 isotopic disequilibrium (Bindeman et al., 2008). We note that melt inclusions such as
325 17pl3a with Mg# > 50 were observed in greater abundance by Métrich et al. (1991); these
326 more primitive melt inclusions may be under-represented in our study. No coherent
327 incompatible element variation is observed to suggest variable degrees of partial melting
328 or fractional crystallization from a single source – for example, TiO_2 does not co-vary
329 with K_2O or total alkalis (Figure 4c). Likewise, B shows no coherent variation with K_2O
330 or total alkalis (Figures 4d and 6a).
331
332 We propose that the apparently random variability in major element compositions is a
333 result of stalling and assimilation of older basaltic units at various depths within the crust
334 beneath Lakagígar. The Tertiary through Holocene basalts underlying Lakagígar may
335 have formed by similar processes and from similar mantle sources, hence the general

336 homogeneity, but at different times and from different magmatic systems such that they
337 need not be identical in composition. Assimilation by the parental Lakagígar magma of
338 different proportions of crustal materials at different depths and with slightly different
339 compositions could explain the uncorrelated major element variations observed in both
340 the melt inclusions and the matrix glasses. The influence of crustal assimilation even
341 within the melt inclusions is supported by the range of Mg#s, which at 43-51 is
342 considerably lower than other OIB-associated melt inclusions (e.g., Mg# = 55-75 in
343 Hawaii, Kobayashi et al., 2004; Mg# up to 88 in Polynesia, Saal et al., 1998).
344
345 *4.1.2 Boron concentrations and isotope ratios*
346 We can compare the melt inclusions and host glasses from Lakagígar with previously
347 analyzed melt inclusions and host glasses from the Reykjanes and Hengill fissure swarms
348 (Gurenko and Chaussidon, 1997), also located in southern Iceland (Figure 1a), on the
349 basis of their B/K_2O ratios and $\delta^{11}B$ (Figure 5). Previous authors have shown that
350 B/K_2O ratios vary between Mid-Ocean Ridge Basalts (MORB) and Ocean Island Basalts
351 (OIB), with lower B/K_2O found in OIB relative to MORB (Figure 5a; Ryan et al., 1996;
352 Chaussidon and Marty, 1995; Chaussidon and Jambon, 1994). Because B and K are
353 believed to have similar partition coefficients during mantle melting (Ryan and
354 Langmuir, 1993), this variability in B/K_2O has been interpreted to represent either
355 fundamental differences in the mantle sources sampled by these two basalt types (Ryan et
356 al., 1996) or addition of B to MORB by assimilation of hydrothermally altered oceanic
357 crust (Chaussidon and Marty, 1995). Geographically, Lakagígar lies in close proximity
358 to the center of the proposed plume (OIB source) beneath Iceland, while Reykjanes is far

359 from the plume, thus presumably more influenced by a MORB-like source (Figure 1a).
360 These assumptions regarding the nature of the mantle sources for magmas at the two
361 volcanic centers are consistent with the B/K_2O ratios, which are more MORB-like in melt
362 inclusions from Reykjanes and more OIB-like in inclusions from Lakagígar (Figure 5a).
363 Hengill, which lies geographically between Reykjanes and Lakagígar, has a range of
364 B/K_2O that spans the difference between the two. The Icelandic melt inclusions as a
365 whole contain some of the lightest boron ratios ever measured in fresh basalts ($\delta^{11}B$ = -8
366 to -14‰ at Reykjanes and Hengill, extending to less than -16‰ at Lakagígar, Figure 5b).
367 All but two of the Lakagígar glasses fall within 2σ of $\delta^{11}B$ values previously measured in
368 Icelandic melt inclusions ($\delta^{11}B$ = -11.3±3.8(2σ)‰; Gurenko and Chausidon 1997), and
369 all but three fall within 2σ of $\delta^{11}B$ values reported for OIB worldwide ($\delta^{11}B$ = -
370 9.9±2.6(2σ)‰; Chaussidon and Marty, 1995). However, the negative correlation
371 between B concentration and $\delta^{11}B$ is a feature unique to Lakagígar.

372

373 On the basis of B/K_2O ratios and the range of $\delta^{11}B$, it may seem at first glance that the
374 Lakagígar melt inclusions simply extend the previous dataset for Iceland to more strongly
375 OIB-influenced values, where the OIB in question is sourced from a mantle plume
376 particularly depleted in ^{11}B. However, the increase of B independently of K_2O is not
377 consistent with variable degrees of melting or crystallization from a single OIB mantle
378 source, nor is it consistent with mixing between MORB and OIB. On a plot of B vs.
379 B/K_2O (Figure 5a), the overall trend for OIB is toward increasing B at a relatively
380 constant B/K_2O of ~3, which reflects the similar partitioning behavior of B and K. The

381 Lakagígar glasses, although they exhibit a range of B/K_2O that is typical of OIB, show a
382 distinct linear correlation between B and B/K_2O, which indicates that B was added
383 independently of K_2O. On the plot of $\delta^{11}B$ vs. B (Figure 5b), the Lakagígar glasses show
384 a trend of decreasing $\delta^{11}B$ with increasing boron concentration, a trend that is not
385 observed in the glasses from Hengill or Reykjanes. The good correlation between B, Li,
386 and $\delta^{11}B$, in the absence of any correlation with K_2O, TiO_2, Mg# (Figures 3 and 5), or
387 P_2O_5 (not shown) suggests that the process controlling B and Li abundances and $\delta^{11}B$ is
388 independent of primary magmatic processes including melt fraction, fractional
389 crystallization, and even mantle source variability. Assimilation of altered basaltic
390 materials in the crust, in which the B and Li abundances are controlled by the extent of
391 alteration rather than primary magmatic processes, would explain the observed
392 correlation between the light elements and $\delta^{11}B$ in the absence of correlation with other
393 incompatible elements.

394

395 It is additionally worth noting that despite the MORB-like B/K_2O in the Reykjanes and
396 some Hengill melt inclusions, the only glasses from Iceland with MORB-like $\delta^{11}B$ are the
397 *host glasses* from Reykjanes (Figure 5). That is, none of the previously analyzed basaltic
398 melt inclusions from Iceland, including those from the presumably MORB-influenced
399 Reykjanes fissure swarm, contain MORB-like $\delta^{11}B$ (Gurenko and Chaussidon, 1997).
400 Thus although the Lakagígar glasses seem to reflect a strongly plume-influenced source
401 relative to Reykjanes and Hengill, the lack of MORB-like boron in any Icelandic melt

inclusions suggests that simple MORB-OIB mixing does not satisfactorily explain the full range of boron behavior.

4.1.3 Volatiles

We observe a weak positive correlation between B and volatile concentrations in the melt inclusions (Figure 4). The general correlation might be interpreted as suggesting that B contents are controlled by B loss during degassing. However, several lines of evidence seem to contradict this interpretation. First of all, the scoriaceous matrix glasses, which are strongly degassed with respect to H_2O, CO_2, and S, have higher B contents than the melt inclusions as a whole. In order to explain the difference in B versus volatile behavior between the melt inclusions and matrix glasses, we would need to call upon very different B partitioning behavior at depth relative to that accompanying shallow-level or syn-eruptive degassing. Secondly, Hervig et al. (2002) report experimental evidence that B is relatively compatible in basaltic liquids relative to aqueous fluid ($D_B^{fluid/melt}$ = 0.33-0.54), and argue that B concentrations in melt inclusions from Cerro Negro volcano show no evidence for significant B loss accompanying degassing of CO_2-H_2O fluids. Finally, Hervig et al. (2002) also show experimentally that the isotopic fractionation factor for B partitioning between melt and fluid is such that the fluid favors heavier B ($1000\ ln\alpha^{melt/fluid}$ = -1.3 to -5.2), which means that the residual magma following boron degassing should have *lower* $\delta^{11}B$ compared to the relatively undegassed parent magma. The trend observed in our data is just the opposite; the melt inclusions with the lowest B (and volatile contents) have the highest $\delta^{11}B$.

Although we may be able to rule out degassing as a controlling factor, interpretation of the volatile concentrations is complicated by possible post-entrapment re-equilibration of volatiles by diffusion through the host phenocryst (this possibility is discussed in more detail in Section 4.5). And even if we take the volatile concentrations at face value (that is, if we assume the concentrations in the melt inclusions represent the concentrations in the magma at the time of entrapment), interpretation of the H_2O-CO2 relationship is not straightforward. The general clustering of the H_2O contents around 0.75 wt% is consistent with open-system degassing, while the lower H_2O contents in inclusions 12pl1a and 12pl1c seem to suggest mixing of components with different volatile contents (Figure 4f). In fact, the two processes may be simultaneously competing for control of the H_2O and CO_2 contents in the magma. Thus we treat the volatile concentrations as interesting supporting evidence, but refrain from drawing hard conclusions based on volatile correlations alone.

An alternative explanation for the correlation between B (and Li) contents, $\delta^{11}B$, and perhaps volatile contents is that isotopically light boron is added together with Li and volatiles by assimilation of hydrothermally altered materials such as palagonite-bearing hyaloclastites or altered basalt flows. The lack of correlation between B and Mg#, total alkalis, and CaO/Al_2O_3, all of which are indices of the degree of melting and/or fractional crystallization, suggests that the processes controlling B, Li, and volatile behavior are decoupled from primary magmatic processes. The overall homogeneity of Lakagígar

446 eruptive products (for example, the almost complete lack of variability in total alkalis vs.
447 silica) suggests that the assimilated material is broadly similar in major element
448 composition to the parental Lakagígar magma. The subtle variations in major element
449 compositions within the melt inclusion suite and between the melt inclusions and the host
450 glasses could reflect subtly different assimilants at different depths beneath the fissure.
451 Although the lower B/K_2O ratios at Lakagígar relative to Reykjanes and Hengill are
452 consistent with a more OIB-like source, the lack of correlation between B or $\delta^{11}B$ with
453 K_2O *within* the Lakagígar suite prevents us from calling upon variable plume input as a
454 clear source of isotopically light B. Assimilation of variably altered basaltic materials,
455 however, could provide a means of adding B, Li, and volatiles independently of any
456 variability (or lack thereof) in bulk composition.

457

458 **4.2 Boron in Icelandic Basalts and Geothermal Fluids**

459 Boron isotope ratios in volcanic glasses from Iceland have been used previously to
460 quantify the extent of assimilation of altered crustal materials in magma compositions
461 ranging from basalts to rhyolites. In the case of basaltic to rhyolitic tephras studied by
462 Rose-Koga and Sigmarsson (2008), crustal assimilation was associated with heavy boron
463 isotope ratios, in contrast to the light boron isotope ratios determined in this study.
464 Isotopically heavy boron is commonly observed in seawater-altered crustal materials. The
465 fractionation factor for boron isotopic distribution between basalt and fluid is such that
466 the rock strongly prefers ^{10}B, while ^{11}B is more enriched in the fluid ($\alpha^{rock/water} = 0.968$;
467 Spivack and Edmond, 1987). Thus basalts that have been altered by hydrothermal

interaction with seawater are isotopically much lighter than the seawater itself – but since seawater is so strongly positive ($\delta^{11}B$ = +39.5‰, Spivack and Edmond, 1987) relative to mantle-derived basalt ($\delta^{11}B$ = -10‰, Chaussidon and Marty, 1995), even with fractionation on the order of -30‰, the seawater-altered basalt will still be isotopically heavier than unaltered basalt (Figure 6; see also Spivack and Edmond, 1987; Smith et al., 1995). Chaussidon and Marty (1995) proposed that while low-temperature hydrothermal alteration of basalt by seawater drives boron isotope ratios toward heavier values, high-temperature hydrothermal alteration by meteoric water drives boron isotope ratios toward lighter values. Meteoric waters have much lighter $\delta^{11}B$ relative to seawater (e.g., $\delta^{11}B$ = -1.8 to +18.2‰ in Icelandic lake waters, Aggarwal et al., 2000). More importantly, during high-temperature alteration involving meteoric waters (for example, when a shallow magmatic system interacts with groundwater, or basaltic lavas are erupted beneath a glacier), B is very soluble in the fluid relative to the basalt and isotopically heavy boron will be stripped away from the rock, leaving the altered basalt with relatively light boron isotopic values. An unavoidable corollary of this conceptual model, however, is that the light boron isotope ratios will be associated with very low B concentrations.

Raffone et al. (2010) report isotopically light boron in altered basalts from the surface to 3 km depth in a geothermal well in the Reykjanes geothermal system (well RN-17 of the Icelandic Deep Drilling Project). They attribute the light boron at depth to hydrothermal alteration by meteoric waters early in the history of the geothermal system, while the currently active geothermal system at Reykjanes has evolved to low-temperature circulation of seawater. This interpretation is supported by oxygen and deuterium

491 isotopic variations observed in hydrothermal minerals from other wells at the Reykjanes
492 geothermal field (Pope et al., 2009). The whole rocks sampled at well RN-17 at 3000 m
493 depth contain 9.27 ppm B with $\delta^{11}B$ = -14.4‰. Altered basalts sampled at the surface
494 contained even lighter boron, with $\delta^{11}B$ = -18.3‰ at a concentration of 3.83 ppm.
495 Raffone et al. (2010) determined by *in situ* SIMS analysis that the primary magmatic
496 minerals in the rocks sampled from 650-3000 m depth within the drillhole contain very
497 little B (~0.01-0.50 ppm in clinopyroxene and plagioclase), and that the boron is
498 concentrated in hydrothermal minerals such as epidote (0.3-9.0 ppm) and amphibole
499 (0.14- 2.3 ppm). Nonetheless, there is insufficient B even in the hydrothermal minerals
500 to account for the high whole rock B concentrations. We infer that the isotopically light
501 boron may be concentrated on altered surfaces within the basalt, which we discuss in
502 detail in Section 4.3.

503

504 Assimilation of altered basalts enriched in isotopically light boron, such as those sampled
505 up to 3 km below the surface at Reykjanes, could explain the relationship between B and
506 $\delta^{11}B$ observed at Lakagígar, independent of major element variation. For example, the
507 altered basalts from below 650 m in well RN-17 contain only ~0.1 wt.% K_2O (Marks et
508 al., 2010), which would be consistent with the lack of correlation between B and K_2O
509 contents in the melt inclusions, if the B addition was by assimilation of similarly altered
510 basalts.

511

512 **4.3 Modeling the Effects of Hydrothermal Alteration**

513 Before we can assess the extent of crustal assimilation in Lakagígar magmas, we must
514 first identify the mantle-derived and crustal end members. With respect to the mantle-
515 derived endmembers, the range of basalts can be distilled down to two representative
516 compositions: OIB ([B] = 1.1 (2σ±1.0) ppm, $\delta^{11}B$ = -9.9 (2σ±2.6)‰; Chaussidon and
517 Marty, 1995) and N-MORB ([B] = 0.5 (2σ±0.2) ppm, $\delta^{11}B$ = -4.0 (2σ±3.2)‰;
518 Chaussidon and Marty, 1995). A few of the melt inclusions and matrix glasses from
519 Lakagígar have $\delta^{11}B$ values outside the range of these endmember basaltic compositions,
520 leaving us in need of an isotopically light mixing endmember. Although one might argue
521 that Iceland is simply characterized by an unusually light OIB source that is variably
522 expressed in the Lakagígar glasses, the addition of B independently of K_2O within the
523 Lakagígar suite (Figure 5a) suggests that the source of light boron may be something
524 more exotic. Bindeman et al. (2006, 2008) suggested that low $\delta^{18}O$ found in eruptive
525 products from Lakagígar results from subsurface stoping, digestion, and devolatilization
526 of hyaloclastites that have been hydrothermally altered by synglacial meltwaters. The
527 case of boron is slightly more complicated than that of oxygen, because low-temperature
528 meteoric waters do not contain enough B to contribute significantly to the water-rock
529 system (e.g., meteoric waters from the Icelandic lakes Myvatn and Thingvallavatn
530 contain <50 ppb B; Aggarwal et al., 2000). If these waters are incorporated into high-
531 temperature hydrothermal systems, however, the boron-depleted fluids will scavenge
532 boron from the basaltic materials through which they flow. The Cl/B ratios found in
533 geothermal waters in the area (~30, on a molal basis; Arnórsson and Andresdottir, 1995)
534 are similar to those measured in the melt inclusions and matrix glasses from Lakagígar,
535 suggesting an intimate relationship between geothermal fluids and basalts with respect to

these elements. High-temperature hydrothermal waters from various locations in Iceland contain, on average, [B] = 3 ppm and $\delta^{11}B$ = -3.7‰, indicating that the extent of isotopic fractionation associated with boron scavenging during this sort of high-temperature fluid-rock interaction is limited to a few permil (Aggarwal et al., 2000).

Although high-temperature hydrothermal fluids from Iceland contain higher concentrations of isotopically light boron relative to low-temperature hydrothermal fluids and meteoric waters (Aggarwal et al., 2000), the partitioning of B between basalt and fluid at high temperatures is such that the fluid will remove B from the rock, rather than adding it. The altered basalts from the Reykjanes geothermal field (Raffone et al., 2010) contain isotopically light boron at uncharacteristically high concentrations for basaltic materials (up to ~12 ppm B). These lavas would have had to have tremendously high initial boron concentrations if the light $\delta^{11}B$ observed today simply reflected loss of heavy boron from an OIB-like basalt with ($\delta^{11}B \approx$ -10‰) during high-temperature interaction with B-poor meteoric waters. We speculate that, as meteorically-derived hydrothermal fluids circulate, they first accumulate boron from interaction with basalt, then cool to a temperature at which the boron can adsorb onto mineral surfaces (e.g., the clay-rich matrix that results from palagonitization of hyaloclastite), with preferential adsorption of ^{10}B relative to ^{11}B (Palmer et al., 1987). Thus, interaction with boron-bearing fluids can potentially drive hyaloclastite or other altered basaltic materials to high B concentrations characterized by low $\delta^{11}B$. The fluids must cool in order for this hypothetical model to function, because if they were to remain at temperatures >200˚C, all of the boron would remain in the fluid rather than adhere to mineral surfaces.

559 Alternatively, isotopically light boron could be taken up directly from meteoric waters
560 during the process of palagonitization. Due to the very low concentration of B in
561 meteoric water, large quantities of water would be required relative to the amount of
562 basalt, which poses thermal limitations. The basaltic lava would likely be quenched
563 before enough meteoric water can be processed to account for the high B concentrations
564 in the altered basalts.
565
566 Let us explore, hypothetically, the B concentrations and $\delta^{11}B$ expected in hyaloclastites
567 or other altered basalts onto which B has been adsorbed from cooling hydrothermal
568 waters. Hyaloclastites are volcanic breccias composed of crystals and glass fragments in
569 a hydrated matrix. They are formed when interaction between hot lava and cold water
570 causes the lava to shatter into mm- to cm- sized shards and ash-like fragments on
571 millisecond timescales in a cyclic process of contact-surface steam explosivity. The water
572 subsequently reacts with the surface of the basaltic glass (sideromelane) to form an
573 altered rind of palagonite. This reaction proceeds at a rate of 2.8 μm per year at 100˚C
574 (Jakobsson and Moore 1997), such that the tiny particles that make up the matrix of the
575 hyaloclastite are altered entirely to palagonite in a relatively short time. Over time the
576 unstable, amorphous palagonite evolves into more organized crystalline structures,
577 ultimately transforming into the clay mineral smectite (Stroncik and Schminke, 2001).
578
579 Quantitatively, the B concentrations and $\delta^{11}B$ will be determined by the adsorption
580 coefficient, the isotopic fractionation factor, and the cumulative water-rock ratio. To
581 calculate the adsorption of boron onto clays in the hyaloclastite matrix, we use values for

582 the adsorption coefficient (K_d = 2.6) and fractionation factor (α = 0.975) determined by
583 Palmer et al. (1987) for adsorption of boron onto marine clays at 25˚C and pH = 7.8. The
584 primary clay mineral in marine clays is illite or mixed-layer illite-smectite, while the clay
585 mineral in hyaloclastites and other altered basalts is smectite, thus we must assume for
586 the purposes of this exercise that adsorption of B onto smectite surfaces is similar to
587 adsorption onto illite surfaces. The isotope ratio in altered hyaloclastite can then be
588 calculated as a function of water-rock ratio (W/R) using the approach of Spivack and
589 Edmond (1987):

590 $$\delta^{11}B_R = \alpha\left(\delta^{11}B_W + 10^3\right)\exp\left[\frac{K_d \cdot (1-\alpha)}{W/R}\right] - 10^3 \qquad \text{Eq. 1}$$

591 where $\delta^{11}B_R$ is the δ^{11}B in the rock, $\delta^{11}B_W$ is the δ^{11}B in the hydrothermal fluid.
592 Analogously, the boron concentration in altered hyaloclastite is given by

593 $$[B]_R = [B]_W \cdot K_d \cdot \exp\left(\frac{-K_d}{W/R}\right) \qquad \text{Eq. 2}$$

594 where $[B]_R$ is the boron concentration in the rock and $[B]_W$ is the boron concentration in
595 the hydrothermal fluid. Model endmembers and results for adsorption of boron onto
596 mineral surfaces in altered basaltic materials are presented in Table 2 and Figure 6. The
597 approach described by Equations 1 and 2 above assumes that all of the boron in the
598 altered rock is derived from the fluid, such that the starting composition of the basalt is
599 inconsequential (that is, the fresh basalt composition could be MORB-like or OIB-like,
600 and the result of this model would be the same). This assumption is valid assuming that
601 the initial boron concentration in the rock is low. We find that modest water/rock ratios of
602 4-10 generate materials with boron concentrations and isotope ratios that are comparable
603 to those of hydrothermally altered basalts from Reykjanes geothermal well RN-17

(Raffone et al., 2010), and make suitable endmembers for crustal assimilation modeling (see Section 4.4). It should be noted that the lack of a modern hydrothermal system at Lakagígar is of no consequence to this conceptual model, as we require simply that there was hydrothermal activity at some time in the history of the Tertiary to Holocene basalts underlying the fissure; this activity may well pre-date by quite some time the eruption of 1783-84.

4.4 Crustal Assimilation Beneath Lakagígar

Figure 7 presents the results of a parabolic mixing model, using as endmembers the Lakagígar melt inclusion with the lowest boron content (12pl1a, $\delta^{11}B$ = -7.8‰, [B] = 0.59 ppm), two representative altered basalts from the Icelandic Deep Drilling Project (one from the surface and one from 3000 m depth in well RN-17; Raffone et al., 2010), and two model altered hyaloclastites onto which boron has been adsorbed from cooled geothermal fluids at water/rock ratios of 4 and 10. Values of mixing endmembers are given in Table 2. Given the existing data, we are unable to predict what the boron concentrations and isotope ratios in a "pure" Icelandic plume melt might be. We have chosen melt inclusion 12pl1a from Lakagígar to represent the background Icelandic mantle source because it overlaps with the previous data from both Reykjanes and Hengill (Gurenko and Chaussidon, 1997). Assuming this composition as representative of the parental magma, the suite of melt inclusions sampled at Lakagígar reflect ~5-15% assimilation of altered crustal materials. The matrix glasses, which represent the bulk of the eruptive products, have assimilated ~15-30% hyaloclastite or altered basalt. These values are consistent with previous estimates for crustal assimilation based on Sr and Th

627 isotope ratios (20%, Sigmarsson and Condomines, 1991), and are within the range of
628 estimates based on oxygen isotope ratios (10-60%; Bindeman et al., 2006, 2008).
629
630 **4.5 Depths of Entrapment**
631 Volatile equilibration pressures were determined using the solubility model of Papale et
632 al (2006), as shown in Figure 4f. The minimum equilibration pressures determined for
633 the melt inclusions on the basis of their measured H_2O and CO_2 concentrations range
634 from ~0.5 to ~1.5 kb. These pressures can be interpreted as entrapment pressures or, if
635 the magma storage time is sufficiently long for H_2O and CO_2 to re-equilibrate by
636 diffusion through the plagioclase host, as the pressure at which the magma was last stored
637 prior to eruption. When volatiles in melt inclusions re-equilibrate subsequent to
638 entrapment, they almost certainly do so at a shallower level (lower pressure) than that at
639 which they were originally trapped. Thus we can reasonably interpret the H_2O-CO_2
640 equilibration pressures as representing *minimum* depths of entrapment, recognizing that
641 the true depths of entrapment may be greater. The volatile equilibration pressures
642 determined here are equal to or less than cotectic (olivine-plagioclase-clinopyroxene)
643 crystallization pressures previously determined for Lakagígar (1.45 kbar; Kelley and
644 Barton, 2008), and considerably less than the maximum crystallization pressures (2.5
645 kbar, Guilbaud et al., 2007; 7.66 kbar, Kelley and Barton, 2008), suggesting that the H_2O
646 and CO_2 in at least some of the melt inclusions may have re-equilibrated by diffusion
647 during magma storage and transport. Alternatively, the H_2O-CO_2 variation in Figure 4f
648 could be interpreted to reflect mixing of relatively volatile-rich and volatile-poor
649 components at under-saturated conditions (in which case the depths of mixing would

650 have to be *greater* than the minimum entrapment depths). Overall, the model
651 equilibration pressures correspond to minimum depths of ~3-4 km, assuming a density of
652 2.5-3.0 g/cm^3 in the overlying crust. These depths are consistent with estimates of the
653 depth to the magma chamber beneath Grímsvötn based on gravity and magnetic methods
654 (1.5-4.0 km; Gudmundsson and Milsom, 1997), geodetic methods (>1.6 km; Sturkell et
655 al., 2003), and teleseismic P-wave delays (3-4 km; Alfaro et al., 2007).
656
657 Geophysical studies of Icelandic magmatic systems over the last two decades have
658 increased our understanding of the storage and migration of magma (e.g. Sturkell et al.
659 2006). These studies indicate that magma migrates from Moho depths (~20 km) to
660 shallower levels (~5 km). The latter also correlates with geodetic estimates of the
661 thickness of the brittle crust along the axes of the neovolcanic zones (e.g., LaFemina et
662 al., 2005; Arnadottir et al., 2009). The March – April 2010 eruption of Eyjafjallakjokull
663 volcano was the end result of approximately two decades of geophysical unrest marked
664 by magmatic intrusion imaged by seismic and geodetic studies (Sigmundsson et al., 2010
665 and references therein). These studies indicate three occurrences of magma intrusion into
666 sills at depths of 4.0 - 6.5 km, where density and strength variations of crustal layers - for
667 example between basaltic lava flows and hyaloclastite or tillite strata - can disrupt the
668 vertical migration of magma and cause sill intrusion (e.g., Taisne and Jaupart, 2009).
669 Our analysis of volatile saturation depths for our plagiocalse-hosted melt inclusions
670 indicates equilibration depths of ~4 km, in agreement with geodetically determined
671 magma chamber depths and upper crustal thicknesses in the Eastern Volcanic Zone. The
672 stalling of magma and horizontal intrusion of sills at contacts between units at these or

673 greater depths, perhaps just beneath the primary magma chamber, would generate the
674 necessary conditions for assimilation of various similar, yet distinct, basaltic
675 compositions, consistent with our observation of subtle, random variability in the major
676 element compositions of the Lakagígar melt inclusions. Variability in B and Li
677 concentrations and $\delta^{11}B$ could be overprinted atop the initial magmatic compositions of
678 these units as a result of hydrothermal alteration prior to assimilation. Figure 8 illustrates
679 the potential magma pathways and accumulation sites in the middle to upper crust
680 beneath Grímsvötn and Lakagígar.
681
682 **4.6 A Recycled Subducted Component in the Plume Source?**
683 We must also consider an alternative explanation – namely, that the source of very low
684 $\delta^{11}B$ in Icelandic magmas is recycled, subducted oceanic crust that has passed through
685 the deep mantle prior to being returned to the surface as a component of the mantle plume
686 presumed to exist beneath Iceland. Some basalts from central Iceland have been
687 interpreted as representing a mantle plume source containing subducted, altered oceanic
688 crust on the basis of isotopic and incompatible trace element characteristics (e.g.,
689 Chauvel and Hémond, 2000; Skovgaard et al., 2001; Gurenko and Chaussidon, 2002;
690 MacPherson et al., 2005). Correlation of moderately isotopically depleted boron ($\delta^{11}B$ as
691 low as -8‰) and oxygen ($\delta^{18}O$ as low as 4.9‰) with radiogenic isotope ratios in basalts
692 from the Azores has been interpreted to reflect the influence of recycled subducted crust
693 in OIB sources (Turner et al. 2007). The relatively low B/K_2O (=1-4) and moderate K_2O
694 wt.% (0.36-0.50) in the Lakagígar glasses suggests a dominantly OIB-like magmatic
695 source. However, the positive correlation of B concentrations with B/K_2O (Figure 5a) is

696 inconsistent with mixing between a MORB-like and an OIB-like source, or with variable
697 melting of a single OIB-like source. In contrast, the B vs. B/K_2O observed in some of the
698 melt inclusions from the Hengill fissure swarm (Gurenko and Chaussidon, 1997) might
699 be explained by MORB-OIB mixing.
700
701 Previous analysis of basaltic melt inclusions from the Reykjanes and Hengill fissure
702 swarms in southwestern Iceland found that the inclusions were characterized by a more
703 or less invariant $\delta^{11}B$ of -11.3 (2σ ±3.8‰) over a range of B concentrations from 0.26-
704 1.42 ppm (Gurenko and Chaussidon, 1997). If we were to exclude the melt inclusions
705 12pl1a and 12pl1c (both hosted in the same phenocryst) from this study, the range of B,
706 K_2O, and $\delta^{11}B$ in the remaining Lakagígar melt inclusions would be generally consistent
707 with the previous data for Reykjanes and Hengill, extending to slightly lower $\delta^{11}B$
708 (Figure 5), and we might be more inclined to consider MORB-OIB mixing. Given the
709 small size of our data set, however, there is no good justification for rejecting two out of
710 six melt inclusions for which we have boron data. As long as we consider all of our data
711 at face value, the trends we observe strongly suggest coherent B, Li, and $\delta^{11}B$ variation
712 that is decoupled from mantle source variation or magmatic processes, and we believe
713 this is most consistent with assimilation of B- and Li- enriched altered crustal materials.
714
715 **4.7 Origin of Volatiles in Lakagígar Magma**
716 If we assume that assimilation of altered crust occurred prior to the 1783-1784 eruption,
717 then it is quite likely that volatile components were added during assimilation of altered
718 materials in addition to boron and lithium. As mentioned previously, we are reluctant to

719 attach too much significance to the observed correlation between boron concentrations
720 and volatile concentrations, as this correlation could potentially be an artifact of post-
721 entrapment effects. Nonetheless, some of the Lakagígar glasses extend to compositions
722 that are clearly enriched in isotopically light boron relative to typical oceanic basalts, and
723 these melt inclusions tend to have higher volatile contents relative to those with lower
724 boron concentrations and more typical isotope ratios. It has been demonstrated
725 previously that Lakagígar lavas and melt inclusions are also enriched in isotopically light
726 oxygen (Hattori and Muehlenbachs,1982; Bindeman et al., 2006; 2008). Palagonites that
727 form the matrix of hyaloclastites such as those that make up Laki Mountain, through
728 which Lakagígar cuts, have variable but high volatile contents (10-20% H_2O; up to 10%
729 CO_2; and up to 1% SO_2; Stroncik and Schminke, 2001). We suggest that the massive
730 quantities of released volatiles that made the 1783-84 Lakagígar eruption so deadly could
731 have originated in altered crustal materials, such as palagonite-rich hyaloclastites, that
732 were assimilated by the magma prior to eruption. The low concentrations of volatiles in
733 the matrix glasses indicate that the volatile components were largely degassed at the time
734 of eruption, leaving behind only the isotopic record of the assimilated materials.
735
736 **5. CONCLUSIONS**
737 Basaltic glasses from the 1783-84 eruption of Lakagígar are characterized by light boron
738 isotope ratios relative to typical oceanic basalts. We have shown that isotopically light
739 boron in fresh basaltic glasses can be explained by subsurface assimilation of very light
740 boron in altered Icelandic basalts, such as those found at depths up to 3 km in well RN-17
741 from the Reykjanes geothermal field (Raffone et al., 2010). We propose a hypothetical

742 model to explain the generation of high concentrations of light boron in altered Icelandic
743 basalts by adsorption onto mineral surfaces from meteorically-derived hydrothermal
744 waters. Mixing models indicate that the range and trend observed in B concentrations
745 and $\delta^{11}B$ at Lakagígar can be produced by assimilation of up to 30% hydrothermally
746 altered crustal materials. This percentage of assimilated material is in agreement with the
747 findings of Sigmarsson and Condomines (1991) based on $^{230}Th/^{232}Th$, [Th], and Th/U in
748 Lakagígar lavas (20% assimilation), and of Bindeman et al. (2008) based on $\delta^{18}O$ in
749 phenocrysts (10-60% assimilation). We propose that the altered crustal component is
750 added during magma migration through sills in the deeper levels of the crust, becoming a
751 ubiquitous feature in the final stages of evolution and mixing in a magma chamber
752 located at ~3-4 km depth, most likely that of the Grímsvötn central volcano. We
753 tentatively suggest that the large mass of volatiles released during the Lakagígar eruption
754 may likewise have originated in part from the assimilation of hyaloclastite and other
755 altered crustal materials at depths of several kilometers beneath the fissure.
756
757 Acknowledgements. The authors wish to thank Mark Angelone and John Cantolina of
758 the PSU Materials Characterization Laboratory (MCL) for their assistance with analyses,
759 and Kari Kristjansson of the Lakagígar Skaftafell National Park for granting access to the
760 tephra deposits. This work was supported by a PSU-EMS Miller Award to MDF, NSF
761 EAR 09117456 to PCL, and awards to MNB by the GSA Northeast Division Grant for
762 Undergraduate Research, the Dept. of Geosciences Undergraduate Senior Thesis Grant,
763 and PSU Undergraduate Research Discovery Grant. This project was inspired by the
764 Center for Advancement of Undergraduate Studies and Experience (CAUSE) field course

765 in Iceland, 2008, sponsored by the College of Earth and Mineral Sciences at PSU. This
766 manuscript was improved by thorough reviews from Stefan Arnorsson and two
767 anonymous reviewers, and by helpful comments from the editor, Steve Shirey.
768

769 **REFERENCES**

770 Aggarwal J., Palmer M., Bullen T., Arnorsson S., and Ragnarsdottir K. (2000) The boron
771 isotope systematic of Icelandic geothermal waters: 1. Meteoric water charged systems.
772 *Geochim. Cosmochim. Acta* **64**, 579-585.
773

774 Alfaro R., Brandsdottir B., Rowlands D., and White R. (2007) Structure of the Grímsvötn
775 central volcano under the Vatnajokull icecap, Iceland. *Geophys. J. Int*. **168** 863-876.
776

777 Arnadottir T., Lund B., Jiang W., Geirsson H., Bjornsson H., Einarsson P., and
778 Sigurdsson T. (2009) Glacial rebound and plate spreading: Results from the first
779 countrywide GPS observations in Iceland. *Geophys. J. Int.* **177** 691-716.
780

781 Arnórsson S. and Andresdottir A. (1995) Processes controlling the distribution of boron
782 and chlorine in natural waters in Iceland. *Geochim. Cosmochim. Acta* **59**, 4125-4146.
783

784 Bell J.D. and Humphries D.J. (1972) Lakagígar fissure eruption. In: *Progress in*
785 *Experimental Petrology*, Nat. Environ. Res. Council, UK Publication Series D2, 110-112.
786

787 Benton L., Tomascak P., and Helz R. (1999) A study of boron isotopes in Kilauea Iki
788 lava lake, Hawaii. *EOS Trans*. *AGU* 80, Fall Meeting Supplement, Abstract V52B-06.
789
790 Bindeman I., Davis A., and Drake M. (1998) Ion microprobe study of plagioclase-basalt
791 partition experiments at natural concentration levels of trace elements. *Geochim.*
792 *Cosmochim. Acta*, **62**, 1175-1193.
793
794 Bindeman I., Gurenko A., Sigmarsson O., and Chaussidon M. (2008) Oxygen isotope
795 heterogeneity and disequilibria of olivine crystals in large volume Holocene basalts from
796 Iceland: Evidence for magmatic digestion and erosion of Pleistocene hyaloclastites.
797 *Geochim. Cosmochim. Acta* **72**, 4397-4420.
798
799 Bindeman I., Sigmarsson O., and Eiler J. (2006) Time constraints on the origin of large
800 volume basalts derived from O-isotopes and trace element mineral zoning and U-series
801 disequilibria in the Lakagígar and Grimsvötn volcanic system. *Earth Planet. Sci. Lett.*
802 **245**, 245-249.
803
804 Chaussidon M. and Jambon A. (1994) Boron content and isotopic composition of oceanic
805 basalts: Geochemical and cosmochemical implications. *Earth Planet. Sci. Lett.* **121**, 277-
806 291.
807
808 Chaussidon M. and Marty B. (1995) Primitive boron isotope composition of the mantle.
809 *Science* **269**, 383-386.

Chaussidon M., Robert F., Mangin D., Hanon P., and Rose E. (1997) Analytical procedures for the measurement of boron isotope compositions by ion microprobe in meteorites and mantle rocks. *J. Geostand. Geoanal*. *Res.* **21**, 7-17.

Chauvel C., and Hémond C. (2000) Melting of a complete section of recycled oceanic crust: trace element and Pb isotopic evidence from Iceland. *Geochem. Geophys. Geosys*. **1,** doi:10.1029/1999GC000002..

Darbyshire F., White R., Priestley K. (2000) Structure of the crust and uppermost mantle of Iceland from a combined seismic and gravity study. *Earth Planet. Sci. Lett.* **181**, 409-428.

Einarsson P. and Sæmundsson K. (1992) Earthquake epicenters 1982–1985 and volcanic systems in Iceland (map). In: *Í hlutarins eðli*. Festschrift for Þorbjörn Sigurgeirsson, ed. Þorsteinn Sigfússon, Menningarsjóður, Reykjavík.

Gudmundsson M. and Milsom J. (1997) Gravity and magnetic studies of the subglacial Grímsvötn Volcano, Iceland; implications for crustal and thermal structure. *J. Geophys. Res*. **102**.

831 Guilbaud M., Blake S., Thordarson T., and Self S. (2007) Role of syn-eruptive cooling
832 and degassing on textures of lavas from the AD 1783-1784 Lakagígar eruption, south
833 Iceland. *J. Petrol*. **48**, 1265-1294.
834
835 Gurenko A. and Chaussidon M. (1997) Boron concentrations and isotopic compositions
836 of the Icelandic mantle: evidence from glass inclusions in olivine. *Chem. Geol*. **135**, 21-
837 34.
838
839 Gurenko A. and Chaussidon M. (2002) Oxygen isotope variations in primitive tholeiites
840 of Iceland: evidence from a SIMS study of glass inclusions, olivine phenocrysts and
841 pillow rim glasses. *Earth Planet Sci. Lett.* **205**, 63−79.
842
843 Hamada M. and Fujii T. (2007) H2O-rich island arc low-K tholeiite magma inferred from
844 Ca-rich plagioclase-melt inclusion equilibria. *Geochem. J*. **41**, 437-461.
845
846 Hattori K., and Muehlenbachs K. (1982) Oxygen Isotope Ratios of the Icelandic Crust. *J.*
847 *Geophys. Res*. **87**, 6559-6565.
848
849 Hauri E., Wang J., Dixon J.E., King P.L, Mandeville C., and Newman S. (2002) SIMS
850 analysis of volatiles in silicate glasses 1: Calibration, matrix effects and comparisons with
851 FTIR. *Chem. Geol*. **183**, 99-114.
852
853 Helo C., Longpré M-A., Shimizu N., Clague D.A., and Stix J. (2011) Explosive eruptions
854 at mid-ocean ridges driven by CO_2-rich magmas. *Nature Geosc*. **4**, 260-263.

Hémond C., Condomines M., Fourcade S., Allegre C., Oskarsson N., and Javoy M. (1988) Thorium, strontium and oxygen isotopic geochemistry in recent tholeiites from Iceland: crustal influence on mantle-derived magmas. *Earth Planet Sci. Lett.* **87**, 273-285.

Hervig R., Moore G., Williams L., Peacock S., Holloway J., and Roggensack K. (2002) Isotopic and elemental partitioning of boron between hydrous fluid and silicate melt. *Am. Mineral.* **87**, 769-774.

Jakobsson S. and Moore J. (1997) Hydrothermal minerals and alteration rates at Surtsey volcano, Iceland. *Geol. Soc. Am. Bull*. **97**, 648-659.

Jochum K.P., Dingwell D.B., Rocholl A., Stoll B., Hofmann A.W., Becker S., Besmehn A., Bessett D., Dietze H.J., Dulski P., Erzinger J., Hellebrand E., Hoppe P., Horn I., Janssens K., Jenner G.A., Klein M., McDonough W.F., Maetz M., Mezger K., Münker C., Nikogosian I.K., Pickhardt C., Raczek I., Rhede D., Seufert H.M., Simakin S.G., Sobolev A.V., Spettel B., Straub S., Vincze L., Wallianos A., Weckwerth G., Weyer S., Wolf D., and Zimmer M. (2000) The preparation and preliminary characterization of eight geological MPI-DING reference glasses for in-situ microanalysis. *Geostand. Newslett.* **24**, 87-133.

877 Kelley D. and Barton M. (2008) Pressures of crystallization of Icelandic magmas. *J.*
878 *Petrol.* **49**, 465-492.
879
880 Kobayashi K., Tanaka R., Moriguti T., Shimizu K., Nakamura E. (2004) Lithium, boron,
881 and lead isotope systematics of glass inclusions in olivines from Hawaiian lavas:
882 evidence for recycled components in the Hawaiian plume. *Chem. Geol.* **212**, 143-161.
883
884 Kress V. and Ghiorso M. (2004) Thermodynamic modeling of post-entrapment
885 crystallization in igneous phases. *J. Volcanol. Geotherm. Res*. **137**, 247-260.
886
887 LaFemina P.C., Dixon T. H., Malservisi R., Árnadóttir E., Sturkell E., Sigmundsson F.,
888 and Einarsson P. (2005) Geodetic GPS measurements in south Iceland: Strain
889 accumulation and partitioning in a propagating ridge system. *J. Geophys. Res*. **110**, 1-21.
890
891 MacPherson C., Hilton D., Day J., Lowry D., and Gronvold K. (2005) High $^{3}He/^{4}He$,
892 depleted mantle and low $\delta^{18}O$ recycled lithosphere in the source of central Iceland
893 magmatism. *Earth Planet Sci. Lett.* **233**, 411-427.
894
895 Marks N., Schiffman P., Zierenberg R.A., Franzson H., Fridleifsson G.Ó. (2010)
896 Hydrothermal alteration in the Reykjanes geothermal system: Insights from Iceland deep
897 drilling program well RN-17. *J. Volcanol. Geotherm. Res.* **189**, 172-190.
898

899 Métrich N., Sigurdsson H., Meyer P., and Devine J. (1991) The 1783 Laki eruption in
900 Iceland: geochemistry, CO_2 and sulfur degassing. *Contrib. Mineral. Petrol*. **107**, 435-447.
901
902 Papale P., Moretti R. and Barbato D. (2006) The compositional dependence of the
903 saturation surface of $H_2O + CO_2$ fluids in silicate melts. *Chem. Geol*. **229**, 78-95.
904
905 Palmer M., Spivack A., and Edmond J. (1987) Temperature and pH controls over isotopic
906 fractionation during adsorption onto marine clays: *Geochim. Cosmochim. Acta*, **51**, 2319-
907 2323.
908
909 Pope E., Bird D., Arnórsson S., Fridriksson T., Elders W.A., Fridleifsson G.Ó. (2009)
910 Isotopic constraints on ice age fluids in active geothermal systems: Reykjanes, Iceland.
911 *Geochim. Cosmochim. Acta* **73**, 4468-4488.
912
913 Pouchou JL. and Pichoir F. (1987) Basic expression of "PAP" computation for
914 quantitative EPMA. In: *Eleventh International Congress on X-Ray Optics and*
915 *Microanalysis,* Ontario University Press, 249-252.
916
917 Raffone N., Ottolini L.P., Tonarini S., Gianelli G., D-Orazio M. and Fridleifsson G.
918 (2010) An investigation of trace and isotope light elements in mineral phases from well
919 RN-17 (Reykjanes Peninsula, SW Iceland). In: *11th European Workshop on Modern*
920 *Developments and Applications in Microbeam Analysis, IOP Conf. Series: Materials*
921 *Science and Engineering* **7**, 012026.

922

923 Rose-Koga E. and Sigmarsson O. (2008) B-O-Th isotope systematics in Icelandic tephra.
924 *Chem. Geol.* **255**, 454-462.

925

926 Rosner M. and Meixner A. (2004) Boron Isotopic Composition and Concentration
927 of Ten Geological Reference Materials. *Geostand. Geoanal. Res*. **28**,431-441.

928

929 Rosner M., Wiedenbeck M., and Ludwig T. (2008) Composition-induced variations in
930 SIMS instrumental mass fractionation during boron isotope ratio measurements of silicate
931 glasses. *Geostand. Geoanal. Res*. **32**, 27-38.

932

933 Ryan J. and Langmuir C. (1993) The systematics of boron abundances in young volcanic
934 rocks. *Geochim. Cosmochim. Acta* **57**, 1489-1498.

935

936 Ryan J., Leeman W., Morris J., Langmuir C. (1996) The boron systematics of intraplate
937 lavas: Implications for crust and mantle evolution. *Geochim. Cosmochim. Acta* **60**, 415-
938 422.

939

940 Saal A., Hart S., Shimizu N., Hauri E., Layne G. (1998) Pb isotopic variability in melt
941 inclusions from oceanic island basalts, Polynesia. *Science* **282**, 1481-1484.

942

943 Sella G., Dixon T., Mao A. (2002), REVEL: A model for recent plate velocities from
944 space geodesy, *J. Geophys. Res.* **107(B4)**, 2081, doi:10.1029/2000JB000033.

945

946 Shimizu K., Shimizu N., Komiya K., Suzuki, K., Maruyama S. and Tatsumi Y. (2009)
947 CO_2-rich komatiitic melt inclusions in Cr-spinels within beach sand from Gorgona Island,
948 Columbia. *Earth Planet. Sci. Lett.* **299**, 33-43.

949

950 Sigmarsson O., and Condomines M. (1991) Extreme magma homogeneity in the 1783-84
951 Lakagígar eruption: origin of large volume of evolved basalt in Iceland. *Geophys. Res.*
952 *Lett*. **18**, 2229-2232.

953

954 Sigmundsson F., Hreinsdottir S., Hooper A., Arnadottir T., Pedersen R., Roberts M.,
955 Oskarsson N., Auriac A., Decriem J., Einarsson P., Geirsson H., Hensch M., Ofeigsson
956 B., Sturkell E., Sveinbjornsson H., and Feigl K. (2010) Intrusion triggering of the 2010
957 Eyjafjallajokull explosive eruption. *Nature* **468**, 426-430.

958

959 Sigurdsson H. and Sparks S. (1978) Rifting Episode in North Iceland in 1874-1875 and
960 the Eruptions of Askja and Sveinagja. *Bull. Volcanol*. **41**, 149-167.

961

962 Skovgaard A.C., Storey M., Baker J., Blusztajn J., and Hart S.R. (2001) Osmium-oxygen
963 isotopic evidence for a recycled and strongly depleted component in the Iceland mantle
964 plume. *Earth Planet. Sci. Lett.* **194**, 259−275.

965

966 Smith H., Spivack A., Staudigel H., and Hart S. (1995) The boron isotopic composition
967 of altered oceanic crust. *Chem. Geol*. **126**, 119-135.

968

969 Spivack A. and Edmond J. (1986) Determination of boron isotope ratios by thermal
970 ionization mass spectrometry of the dicesium metaborate cation. *Anal. Chem.* **58**, 31-35.
971

972 Spivack A. and Edmond J. (1987) Boron isotope exchange between seawater and the
973 oceanic crust. *Geochim. Cosmochim. Acta*, **51**, 1033-1043.
974

975 Stroncik N., and Schminke H. (2001) Evolution of palagonite: Crystallization, chemical
976 changes and elemental budget. *Geochem. Geophys. Geosys*. **2**, 1-43.
977

978 Sturkell E., Einarsson P., Sigmundsson F., Hreinsdottir F., and Geirsson H. (2003)
979 Deformation of Grímsvötn volcano, Iceland: 1998 eruption and subsequent inflation.
980 *Geophys. Res. Lett*. **30**, 1182.
981

982 Sturkell E., Einarsson P., Sigmundsson F., Geirsson H., Olafsson H., Pedersen R., de
983 Zeeuw-van Dalfsen E., Linde A.T., Sacks I.S., and Stefansson R. (2006) Volcano
984 geodesy and magma dynamics in Iceland. *J. Volcanol. Geotherm. Res*. **150**, 14-34.
985

986 Sun S-S. and McDonough W. (1995) Chemical and isotopic systematics of oceanic
987 basalts: Implications for mantle composition and processes. In: Saunders A, Norry M
988 (eds) Magmatism in ocean basins. *Geol. Soc. Spec. Publ.* **42**, 313-345.
989

990 Taisne B. and Jaupart C. (2009) Dike propagation through layered rocks. *J. Geophys.*
991 *Res*. **114**.
992
993 Thorarinsson S. (1979) On the damage caused by volcanic eruptions with special
994 reference to tephra and gases. In: *Volcanic Activity and Human Ecology*, 125-159.
995
996 Thordarson T., and Self S. (1993) The Laki (Skaftár Fires) and Grímsvötn eruptions in
997 1783-1785. *Bull. Volcanol*. **55**, 233-263.
998
999 Thordarson T., Self S., Óskarsson N., and Hulsebosch T. (1996) Sulfur, chlorine and
1000 fluorine degassing and atmospheric loading by the 1784-1784 AD Laki (Skaftár Fires)
1001 eruption in Iceland. *Bull. Volcanol*. **58**, 205-225.
1002
1003 Tilling R.I. (1996) Hazards and climatic impact of subduction zone volcanism: A global
1004 and historical perspective. In: *Subduction Top to Bottom*. *Geophysical Monograph* **96**,
1005 American Geophysical Union.
1006
1007 Turner S., Tonarini S., Bindeman I., Leeman W., and Schaefer B. (2007) Boron and
1008 oxygen isotope evidence for recycled components over the past 2.5 Gyr. *Nature* **447**,
1009 702-705.
1010
1011

1012

1013 **FIGURES**

1014 **Figure 1:** a) Map of Iceland. NA = North American Plate; EU = European Plate; EVZ =
1015 Eastern Volcanic Zone; WVZ = Western Volcanic Zone; NVZ = Northern Volcanic
1016 Zone. Contours are depth to Moho (km) from Darbyshire et al., 2000. The 40 km
1017 contour is assumed to correspond to the center of the Icelandic plume. Dashed box
1018 delineates the area expanded in Figure 1b. The Reykjanes, Hengill, and Lakagígar fissure
1019 swarms are marked with solid stars. Shaded gray areas are fissure swarm locations from
1020 Einarsson and Sæmundsson, 1992. Spreading rate of 19.8 mm/yr from Sella et al., 2002.
1021 b) Location of Lakagígar (Laki Fissure) in southeastern Iceland. The grey region marks
1022 the extent of lava flows from the 1783-1784 eruption. Inverted triangles indicate sample
1023 locations, and open circles indicate locations of two tuff cones presumed to be the
1024 sources of the phreatomagmatic tephra deposits.

1025 **Figure 2:** Examples of basalt glass types analyzed. a) Transmitted light photomicrograph
1026 of melt inclusions in crystal 14pl2; b) Secondary electron image of a tephra clast (LG-
1027 0808-8.2) in cross section, showing the locations of plagioclase microlites.

1028 **Figure 3:** Selected major and trace element concentrations and $\delta^{11}B$ in Lakagígar melt
1029 inclusions and host glasses. a) Mg/(Mg+Fe)x100 vs. TiO_2 wt.%; b) Mg/(Mg+Fe)x100
1030 vs. CaO/Al_2O_3; c) (Na_2O+K_2O) wt.% vs. TiO_2 wt.%; d) (Na_2O+K_2O) wt.% vs. B ppm; e)
1031 Li ppm vs. B ppm; f) $\delta^{11}B$ vs. B ppm. Selected "end-member" melt inclusions for
1032 various elemental concentrations, ratios, or $\delta^{11}B$ values are labeled. Error bars are
1033 average 2σ external reproducibilities based on replicate analysis of unknowns; internal
1034 errors are comparable. Solid error bars apply to analyses performed using the Cameca

1035 ims 1280, and dashed error bars apply to analyses performed using the Cameca ims 3f.
1036 In general, melt inclusions were analyzed by 1280 and host glasses were analyzed by 3f.
1037 See Table 1 for actual uncertainties for each data point.

1038 **Figure 4:** Volatile concentrations plotted against boron concentrations in melt inclusions
1039 (closed symbols) and host glasses (open symbols). a) H_2O wt.% vs. B ppm; b) CO_2 ppm
1040 vs. B ppm; c) S ppm vs. B ppm; d) F ppm vs. B ppm; e) Cl ppm vs. B ppm; f) H_2O wt.%
1041 vs. CO_2 ppm. Isobars on the plot of H_2O vs. CO_2 represent minimum entrapment
1042 pressures, and are calculated using the volatile saturation model of Papale et al. (2006).
1043 Error bars are average 2σ external reproducibilities based on replicate analysis of
1044 unknowns; internal errors are about an order of magnitude less. Solid error bars apply to
1045 analyses performed using the Cameca ims 1280, and dashed error bars apply to analyses
1046 performed using the Cameca ims 3f. In general, melt inclusions were analyzed by 1280
1047 and host glasses were analyzed by 3f (for B concentrations only – all volatiles by 1280).
1048 See Table 1 for actual uncertainties for each data point.

1049 **Figure 5:** B/K_2O, B, and $\delta^{11}B$ in scoria matrix glasses (open symbols) and melt
1050 inclusions (closed symbols). a) B vs. B/K_2O; b) B vs. $\delta^{11}B$. Lakagígar glasses (this
1051 study) are shown as circles, and glasses from the Hengill and Reykjanes fissure swarms
1052 (Gurenko and Chaussidon, 1997) are shown as squares and triangles, respectively, for
1053 comparison. Error bars represent 2σ uncertainty. When replicate analysis was possible,
1054 errors shown represent external reproducibility, otherwise errors represent internal
1055 precision. For boron concentrations and isotope ratios, internal and external uncertainties
1056 were essentially the same. Dashed error bars indicate boron concentrations determined by
1057 Cameca ims 3f, all other data collected by Cameca ims 1280. Medium gray field

represents range of OIB from the literature: Chaussidon and Jambon, 1994; Chaussidon and Marty, 1995; Ryan et al., 1996; Turner et al., 2007. Dark gray field represents range of N-MORB from Chaussidon and Jambon, 1994.

Figure 6: Effects of water-rock interaction on boron concentrations and isotope ratios in mid-ocean ridge basalts (MORB) and meteoric water. Solid lines with arrows indicate trend of low-temperature basalt alteration by seawater (upper trend) or adsorption of boron from cooled, glacially-derived, geothermal fluids (lower trend). Tick marks on lower trend indicate the water/rock ratio during adsorption. Alteration of OIB or "typical" Icelandic basalt would follow a similar trend starting from slightly higher [B] and lower $\delta^{11}B$. Dashed line with arrow depicts the trend of boron enrichment in meteoric (glacial) water as a result of high-temperature water-rock interaction. Closed symbols represent basalts, open symbols represent waters. Data sources given in Table 2.

Figure 7: Results of parabolic mixing model using the Lakagígar melt inclusion with the lowest B concentration (12pl1a) as a starting point, and either model altered hyaloclastite (this study) or actual altered Icelandic basalts as endmembers. Model altered hyaloclastite compositions are calculated assuming that B is adsorbed onto the surface of palagonite during hydrothermal circulation at water-rock ratios of 4 and 10. Actual basalt compositions are whole rock analyses of samples collected at the surface and at 3000m depth in geothermal well RN-17, Reykjanes geothermal field (Raffone et al., 2010). Endmember values for mixing model are given in Table 2. Tick marks indicate 5% or 10% increments of altered crust assimilation. Closed symbols represent melt inclusions, open symbols represent matrix glasses. Error bars are average 2σ external reproducibilities based on replicate analysis of unknowns; internal errors are comparable.

1081 Solid error bars apply to analyses performed using the Cameca ims 1280, and dashed
1082 error bars apply to analyses performed using the Cameca ims 3f. In general, melt
1083 inclusions were analyzed by 1280 and host glasses were analyzed by 3f. See Table 1 or
1084 Figure 5b for actual uncertainties for each data point.
1085 **Figure 8:** Illustration of the magma plumbing system beneath Lakagígar showing the
1086 development of sills at boundaries of density contrast (i.e., between lava flows and
1087 hyaloclastites) at mid- to deep- crustal levels beneath the Grímsvötn magma chamber.
1088 Assimilation of hydrothermally altered materials within these sills contributes
1089 isotopically light boron to the magma, accompanied by subtle variations in major element
1090 compositions. Mixing in the magma chamber beneath the central volcano homogenizes
1091 the magma prior to the fissure eruption.
1092

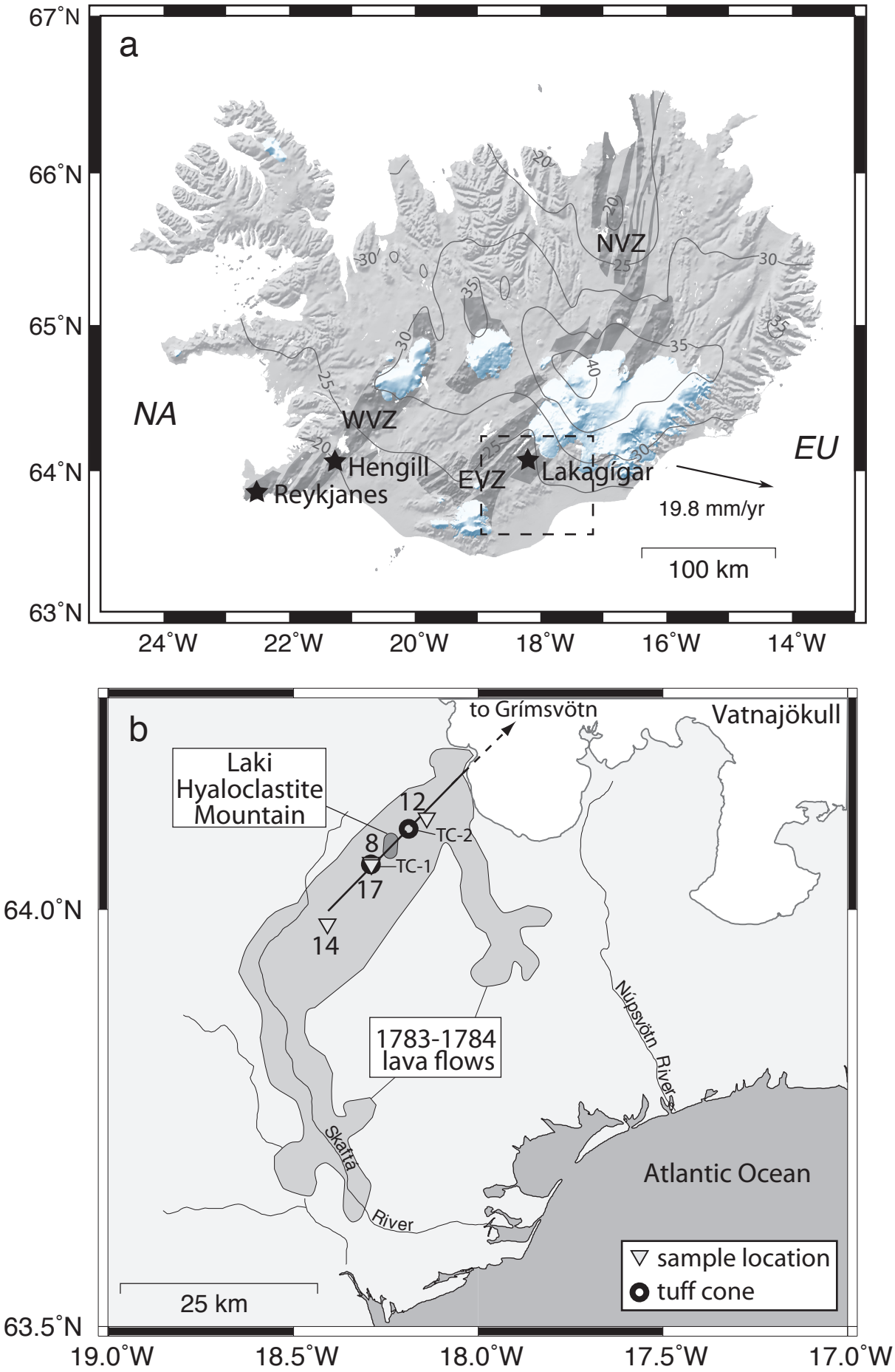
a
67°N
66°N
65°N
64°N
63°N
24°W
22°W
20°W
18°W
16°W
14°W
NA
EU
NVZ
WVZ
EVZ
Hengill
Reykjanes
Lakagígar
19.8 mm/yr
100 km
b
64.0°N
63.5°N
19.0°W
18.5°W
18.0°W
17.5°W
17.0°W
to Grímsvötn
Vatnajökull
Laki
Hyaloclastite
Mountain
12
TC-2
8
TC-1
17
14
1783-1784
lava flows
Núpsvötn River
Skaftá
River
Atlantic Ocean
sample location
tuff cone
25 km

Figure 1

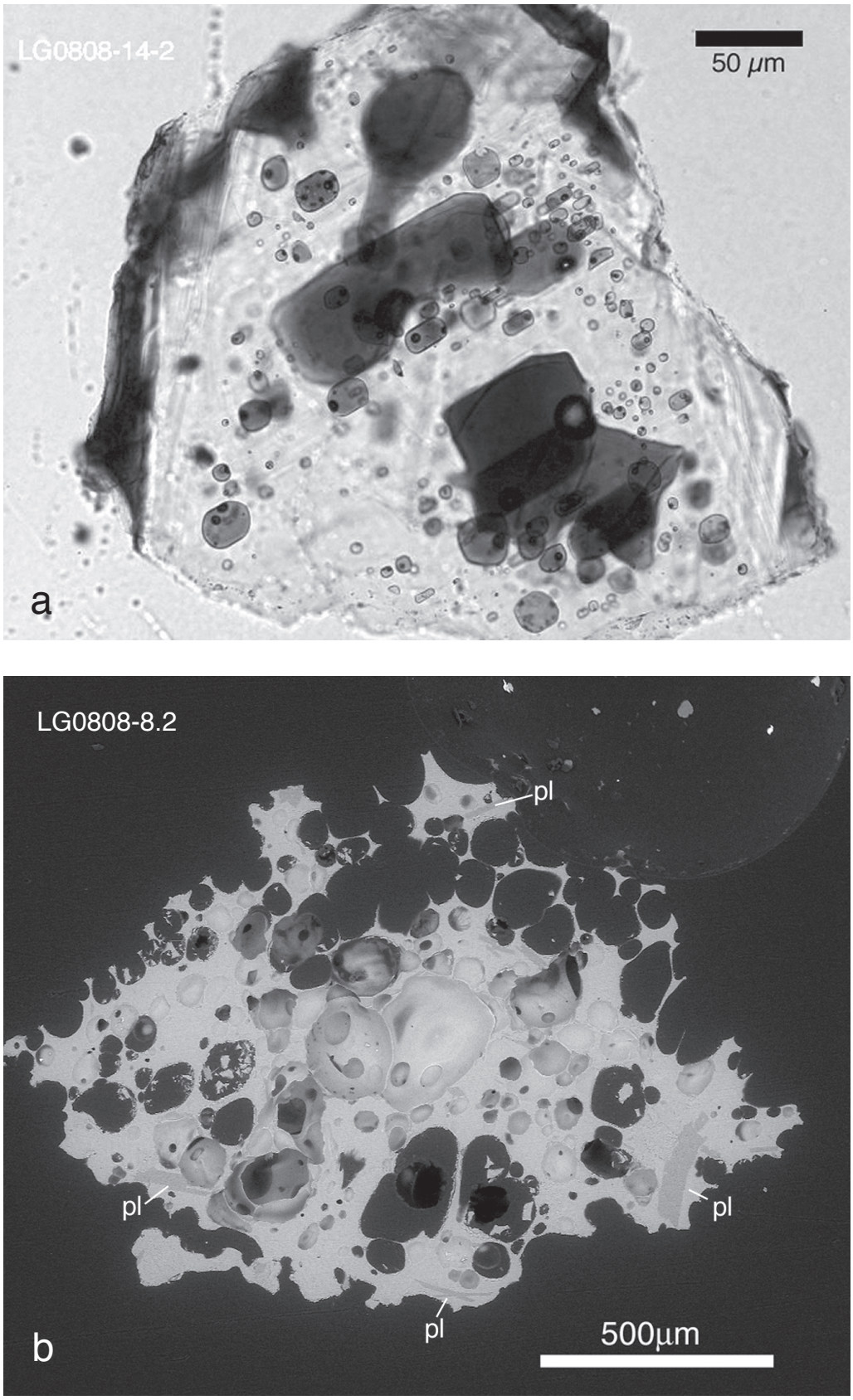

Figure 2

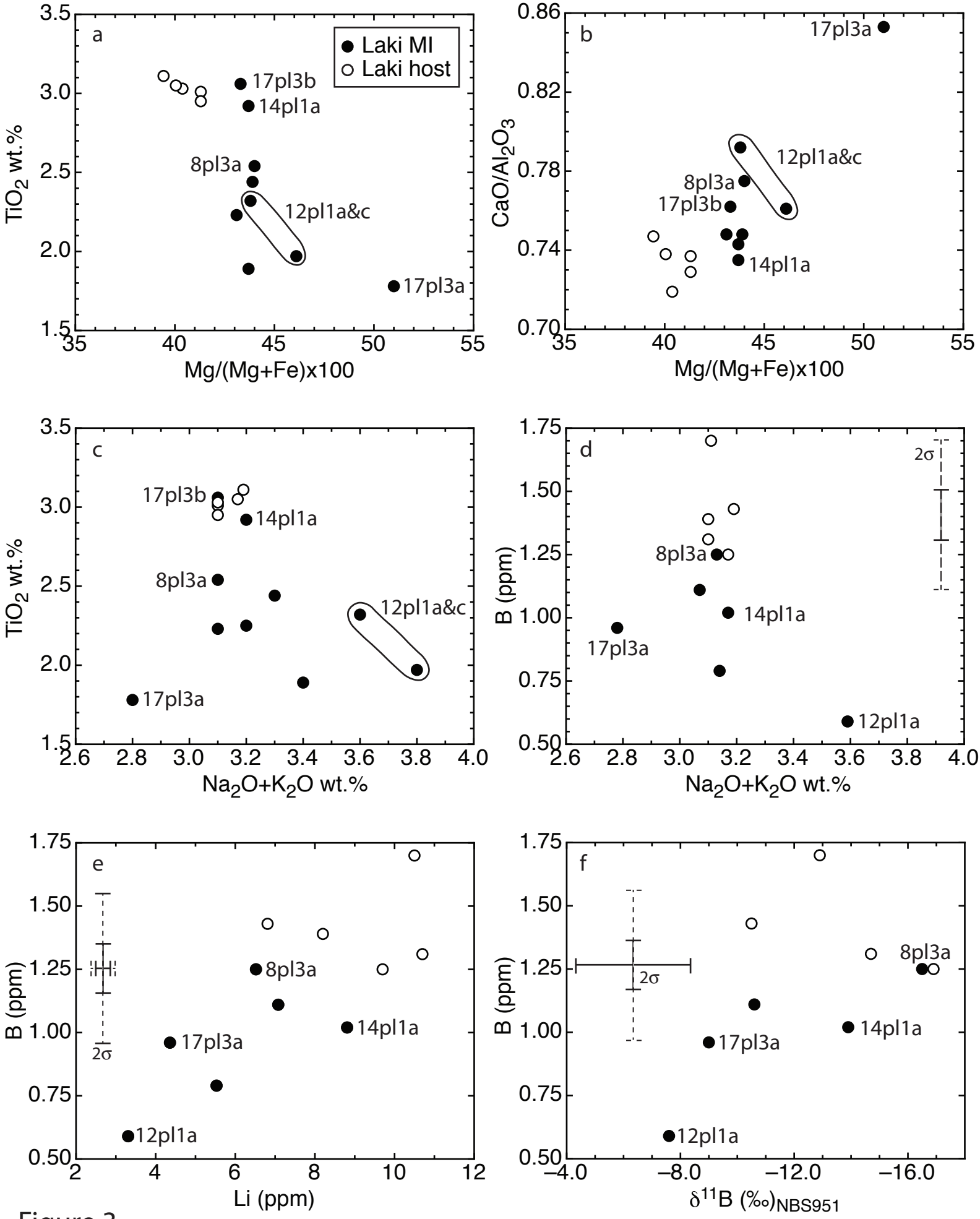
a
Laki MI
Laki host
17pl3b
14pl1a
8pl3a
12pl1a&c
17pl3a
TiO2 wt.%
Mg/(Mg+Fe)x100
b
17pl3a
12pl1a&c
8pl3a
17pl3b
14pl1a
CaO/Al2O3
Mg/(Mg+Fe)x100
c
17pl3b
14pl1a
8pl3a
12pl1a&c
17pl3a
TiO2 wt.%
Na2O+K2O wt.%
d
2σ
8pl3a
14pl1a
17pl3a
12pl1a
B (ppm)
Na2O+K2O wt.%
e
8pl3a
14pl1a
17pl3a
12pl1a
2σ
B (ppm)
Li (ppm)
f
8pl3a
2σ
14pl1a
17pl3a
12pl1a
B (ppm)
δ11B (‰)NBS951

Figure 3

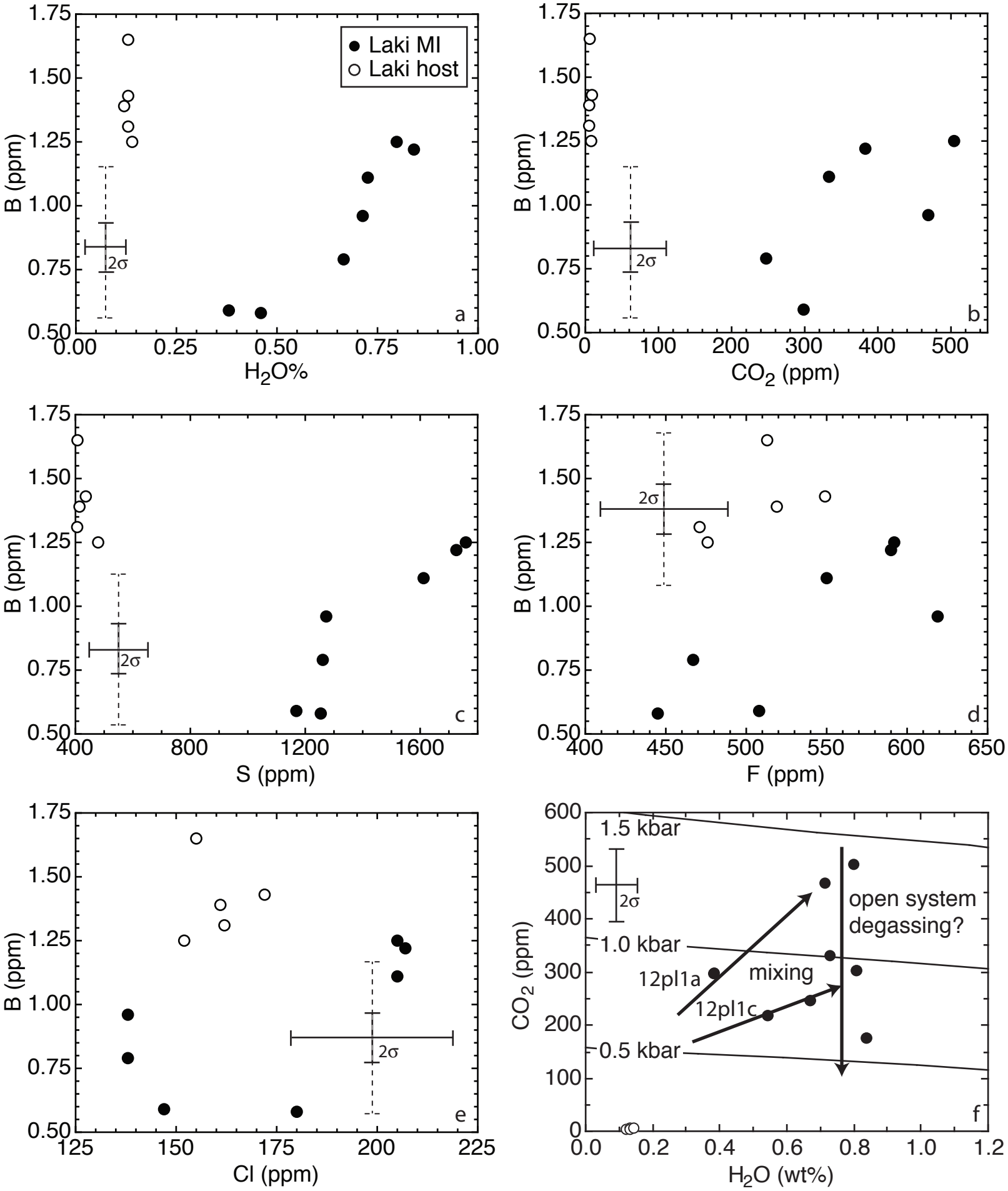
Laki MI
Laki host
B (ppm)
H2O%
CO2 (ppm)
S (ppm)
F (ppm)
Cl (ppm)
CO2 (ppm)
H2O (wt%)
2σ
a
b
c
d
e
f
1.5 kbar
1.0 kbar
0.5 kbar
12pl1a
12pl1c
mixing
open system
degassing?

Figure 4

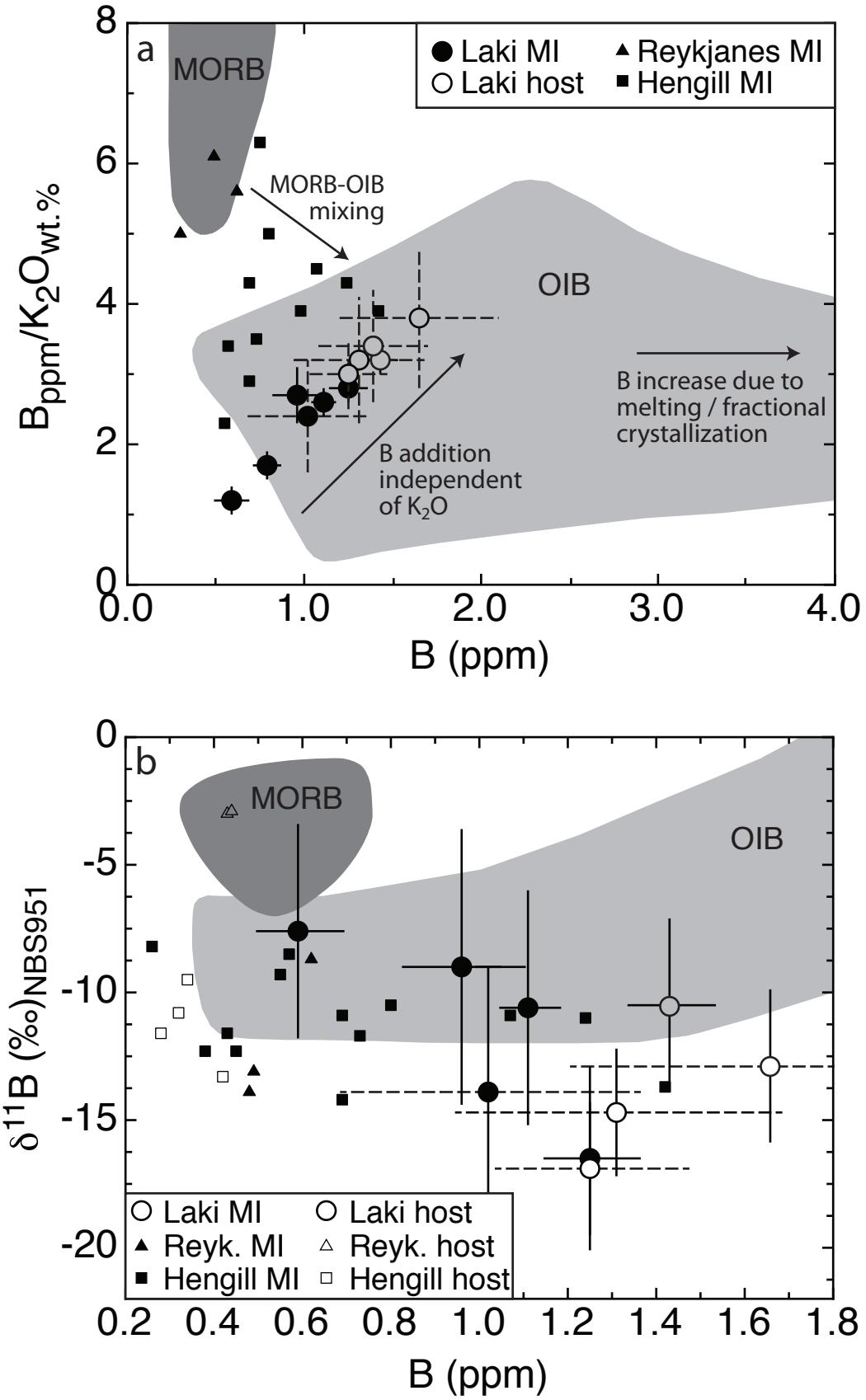
a
MORB
Laki MI
Laki host
Reykjanes MI
Hengill MI
MORB-OIB mixing
OIB
B increase due to melting / fractional crystallization
B addition independent of K2O
Bppm/K2Owt.%
B (ppm)
b
MORB
OIB
Laki MI
Laki host
Reyk. MI
Reyk. host
Hengill MI
Hengill host
δ11B (‰)NBS951
B (ppm)

Figure 5

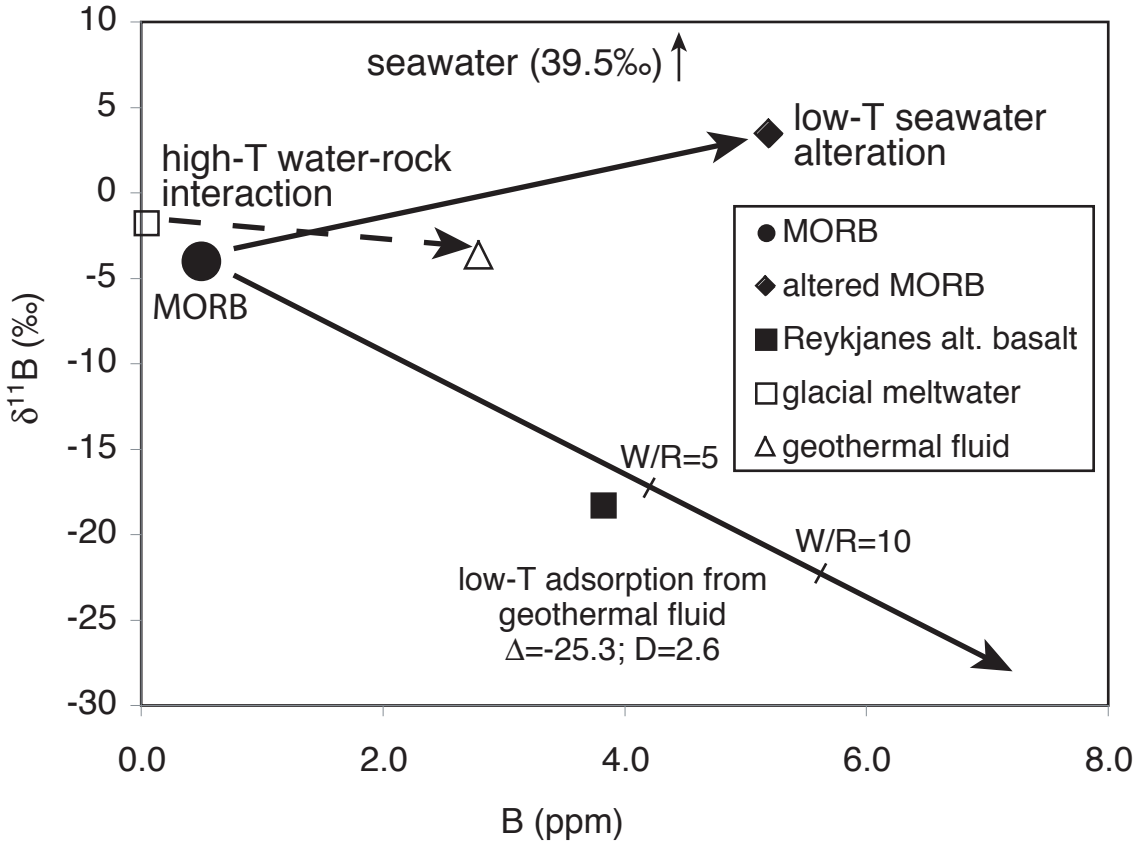
10
5
0
-5
-10
-15
-20
-25
-30
0.0
2.0
4.0
6.0
8.0
B (ppm)
δ11B (‰)
seawater (39.5‰)
low-T seawater alteration
high-T water-rock interaction
MORB
MORB
altered MORB
Reykjanes alt. basalt
glacial meltwater
geothermal fluid
W/R=5
W/R=10
low-T adsorption from geothermal fluid
Δ=-25.3; D=2.6

Figure 6

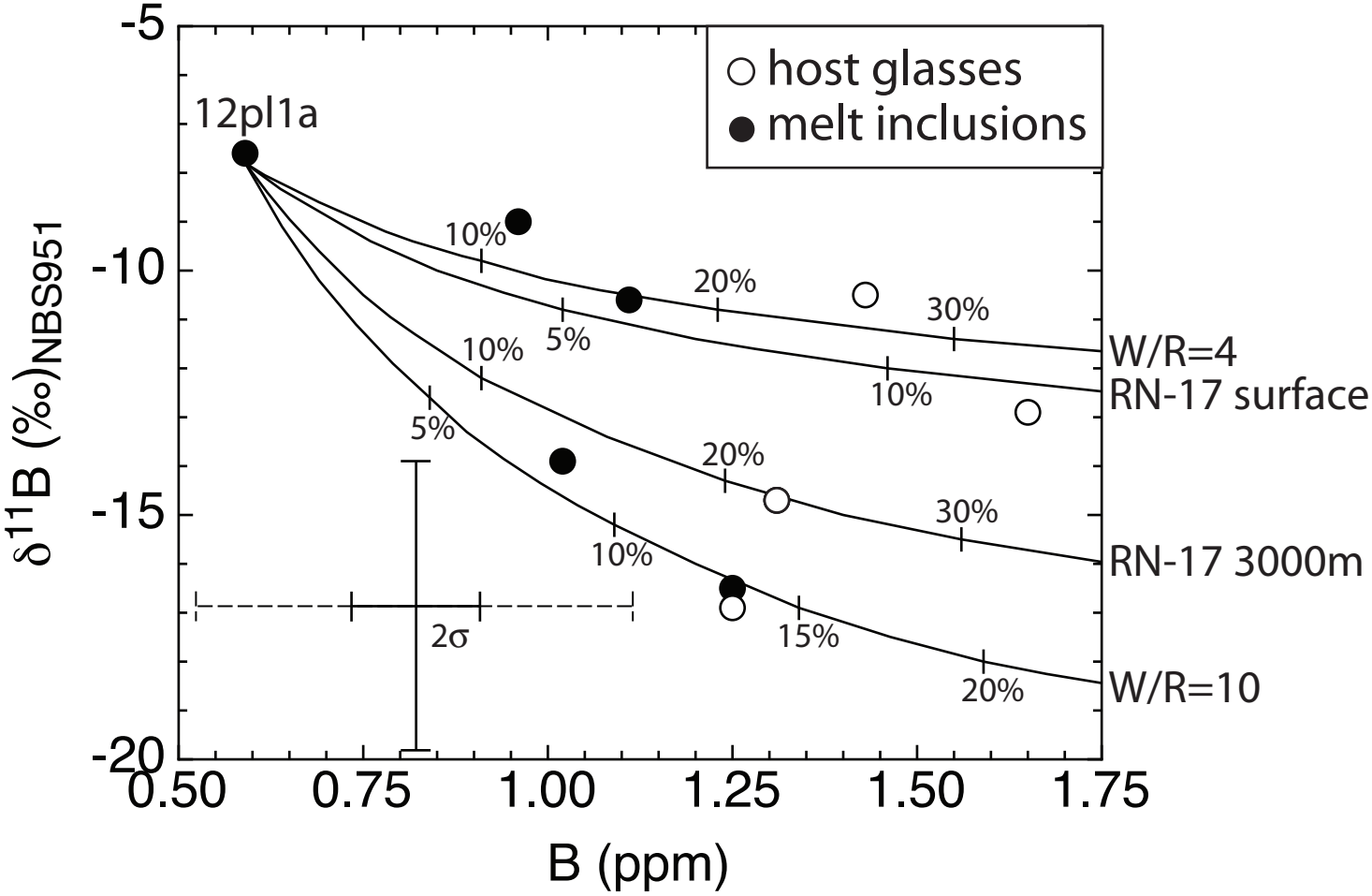
host glasses
melt inclusions
12pl1a
10%
5%
20%
30%
W/R=4
RN-17 surface
10%
5%
10%
20%
30%
RN-17 3000m
10%
15%
20%
W/R=10
2σ
-5
-10
-15
-20
0.50
0.75
1.00
1.25
1.50
1.75
B (ppm)
δ11B (‰)NBS951

Figure 7

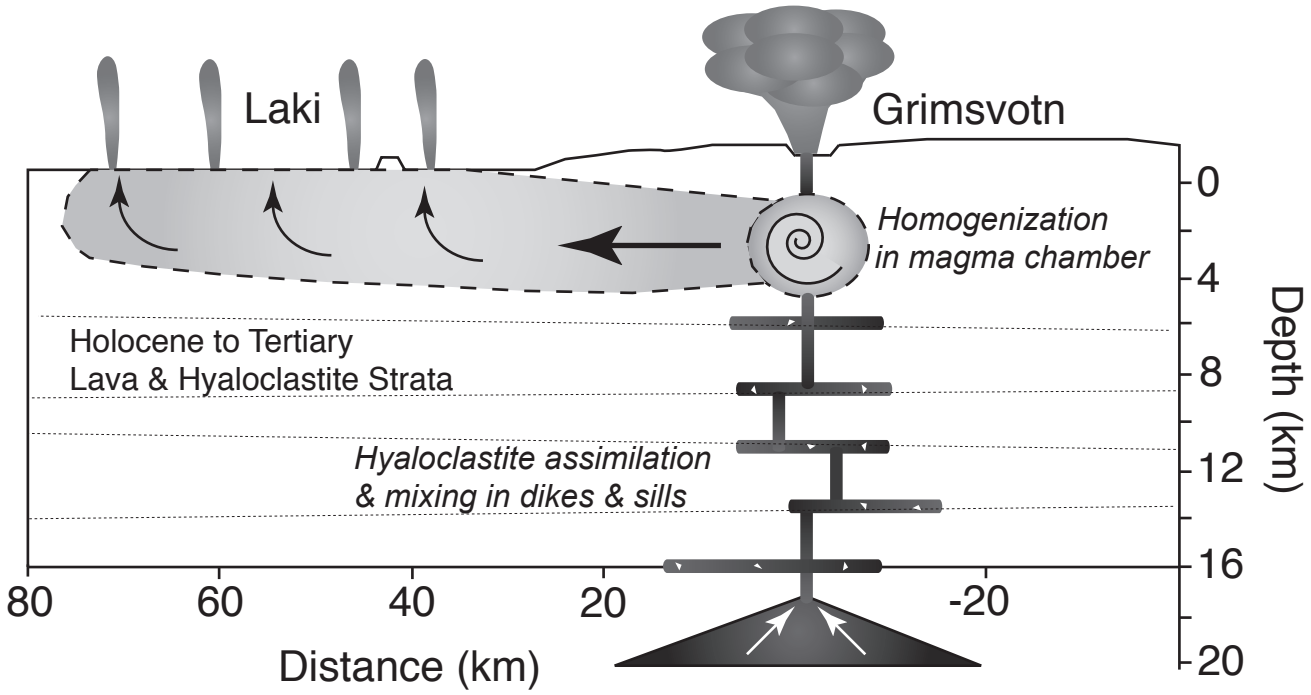
Laki
Grimsvotn
Homogenization
in magma chamber
Holocene to Tertiary
Lava & Hyaloclastite Strata
Hyaloclastite assimilation
& mixing in dikes & sills
80
60
40
20
-20
Distance (km)
0
4
8
12
16
20
Depth (km)

Figure 8

Table 1. Major elements, B concentrations, $\delta^{11}B$, and volatile contents in plagioclase-hosted melt inclusions and matrix glasses

	Matrix Glass					*Melt Inclusions*	
Sample #	LG-0808-8.2	LG-0808-8.4	LG-0808-12	LG-0808-14	LG-0808-17	LG-0808-8	LG-0808-12
Crystal/incl.						pl3a	pl1a
SiO_2	50.01	50.01	49.32	49.11	49.86	48.42	49.15
TiO_2	2.93	2.89	3.02	2.94	3.00	2.45	2.27
Al_2O_3	12.84	12.93	12.51	12.90	12.92	12.53	12.31
FeO*	13.45	13.82	14.10	13.93	14.04	13.54	13.93
MnO	0.23	0.20	0.19	0.22	0.26	0.21	0.23
MgO	5.32	5.24	5.15	5.29	5.26	5.97	6.09
CaO	9.36	9.52	9.34	9.28	9.53	9.71	9.76
Na_2O	2.61	2.63	2.65	2.60	2.69	2.58	3.01
K_2O	0.42	0.41	0.45	0.41	0.42	0.45	0.50
P_2O_5	0.25	0.27	0.31	0.26	0.25	0.28	0.12
Total	97.42	97.91	97.04	96.94	98.23	96.14	97.37
Mg# in glass	41	40	39	40	40	44	44
An% in host	---	---	---	---	---	83	85
B (ppm)	1.65[a]	1.39[a]	1.43	1.31[a]	1.25[a]	1.25	0.59
2σ[b]	0.45 (n=1)	0.31 (n=2)	0.10 (n=2)	0.37 (n=1)	0.22 (n=2)	0.11 (n=1)	0.10 (n=1)
Li (ppm)	10.5 [a]	8.20 [a]	6.81	10.7 [a]	9.70 [a]	6.52	3.31
2σ[b]	1.4 (n=1)	1.57 (n=2)	0.40 (n=2)	1.57 (n=1)	0.38 (n=2)	0.45 (n=1)	0.44 (n=1)
$\delta^{11}B$ ‰	-12.9	nd	-10.5	-14.7	-16.9	-16.5	-7.8
2σ[b]	3.0 (n=1)	---	3.4 (n=1)	2.5 (n=2)	4.1 (n=2)	3.6 (n=1)	4.2 (n=1)
H_2O%	0.13	0.12	0.13	0.13	0.14	0.80	0.38
2σ[b]	0.00 (n=1)	0.03 (n=2)	0.01 (n=2)	0.06 (n=2)	0.07 (n=4)	0.07 (n=2)	0.03 (n=2)
CO_2 (ppm)	5.9	5.2	4.2	5.1	5.2	504	298
2σ[b]	0.8 (n=1)	2.2 (n=2)	1.2 (n=1)	2.4 (n=1)	5.2 (n=3)	44 (n=2)	93 (n=2)
S (ppm)	407	414	436	406	479	1759	1169
2σ[b]	3 (n=1)	31 (n=2)	71 (n=2)	21 (n=2)	185 (n=4)	247 (n=2)	87 (n=2)
Cl (ppm)	155	161	172	162	152	205	147
2σ[b]	1 (n=1)	6 (n=2)	26 (n=2)	1 (n=2)	27 (n=4)	32 (n=2)	11 (n=2)
F (ppm)	513	519	549	471	476	592	508
2σ[b]	3 (n=1)	21 (n=2)	55 (n=2)	33 (n=2)	75 (n=4)	57 (n=2)	39 (n=2)

Table 1 cont'd. Major elements, B concentrations, $\delta^{11}B$, and volatile contents in plagioclase-hosted melt inclusions and matrix glasses

	Melt Inclusions						
Sample #	LG-0808-12	LG-0808-14	LG-0808-14	LG-0808-14	LG-0808-14	LG-0808-17	LG-0808-17
Crystal/incl.	pl1c	pl1a	pl2a	pl2c	pl2d	pl3a	pl3b
SiO_2	50.60	49.20	48.74	50.08	49.90	49.00	49.61
TiO_2	1.95	2.85	2.14	1.85	2.38	1.73	2.98
Al_2O_3	12.68	13.01	12.87	12.86	12.76	12.68	12.34
FeO*	13.27	13.06	13.06	13.34	13.24	12.15	13.52
MnO	0.26	0.21	0.18	0.21	0.24	0.22	0.24
MgO	6.36	5.68	5.56	5.81	5.82	7.09	5.79
CaO	9.66	9.57	9.62	9.55	9.54	10.82	9.41
Na_2O	3.29	2.67	2.51	2.81	2.70	2.34	2.59
K_2O	0.44	0.42	0.42	0.49	0.49	0.36	0.47
P_2O_5	0.17	0.25	0.22	0.14	0.24	0.18	0.35
Total	98.68	96.92	95.32	97.14	97.31	96.57	97.30
Mg# in glass	46	44	43	44	44	51	43
An% in host	85	76	84	84	84	88	88
B (ppm)	nd	1.02[a]	1.11	nd	nd	0.96	0.79
2σ[b]	---	0.34 (n=1)	0.07 (n=1)	---	---	0.14 (n=1)	0.08 (n=1)
Li (ppm)	nd	8.81[a]	7.08	nd	nd	4.36	5.53
2σ[b]	---	1.42 (n=1)	0.41 (n=1)	---	---	0.21 (n=1)	0.41 (n=1)
$\delta^{11}B$ ‰	nd	-13.9	-10.6	nd	nd	-9.0	nd
2σ[b]	---	4.9 (n=1)	4.6 (n=1)	---	---	5.4 (n=1)	---
H_2O%	0.54	nd	0.83	0.80	0.84	0.71	0.67
2σ[b]	0.01 (n=1)	---	0.01 (n=1)	0.01 (n=1)	0.01 (n=1)	0.02 (n=1)	0.04 (n=2)
CO_2 (ppm)	220	nd	333	303	178	469	247
2σ[b]	28 (n=1)	---	10 (n=1)	8 (n=1)	6 (n=1)	12 (n=1)	102 (n=2)
S (ppm)	1497	nd	1713	1587	1668	1273	1261
2σ[b]	14 (n=1)	---	14 (n=1)	12 (n=1)	16 (n=1)	17 (n=1)	86 (n=2)
Cl (ppm)	203	nd	195	189	188	138	138
2σ[b]	7 (n=1)	---	2 (n=1)	2 (n=1)	3 (n=1)	3 (n=1)	11 (n=2)
F (ppm)	600	nd	624	580	579	619	467
2σ[b]	4 (n=1)	---	4 (n=1)	5 (n=1)	5 (n=1)	9 (n=1)	45 (n=2)

Major elements presented as oxide weight percent; analyses conducted using the Cameca SX-50 in the Materials Characterization Laboratory, Penn State.
Unless otherwise indicated, trace element, isotope ratio, and volatile analyses conducted using the Cameca IMS 1280 at NENIMF (WHOI).
nd = not determined for this sample.

(a) Boron and lithium concentrations by Cameca IMS 3f at NENIMF (WHOI).

(b) When n=1, reported uncertainties are internal precision. When n>1, reported uncertainties are the greater of the external reproducibility and internal precision (in most cases this will be the external reproducibility). All uncertainties reported as 2 standard deviations of the mean (95% confidence).

Table 2. Mixing model endmembers and reference values

Endmember	B (ppm)	$d^{11}B$ (‰)	Reference
Mixing model endmembers			
Low-B Lakagígar melt inclusion (12pl1a)	0.59	-7.8	This study
Altered Reykjanes basalt,' surface flow	3.83	-18.3	Raffone et al., 2010
Altered Reykjanes basalt,' 3000m depth (geothermal well)	9.27	-14.4	Raffone et al., 2010
Model adsorbed boron on altered basalt[a]			
Water/rock = 4	3.8	-12.7	This study
Water/rock = 10	5.6	-22.3	This study
Reference values			
N-MORB	0.5	-4	Chaussidon and Marty, 1995
Seawater altered MORB	5.2	+3.4	Smith et al., 1995
Glacial meltwater (meteoric)[b]	0.05	-1.8	Aggarwal et al., 2000
Icelandic geothermal water[c]	2.8	-3.7	Aggarwal et al., 2000
Seawater	4.6	+39.5	Spivack and Edmond, 1987

[a] Model for boron absorbed onto clay-like alteration products using an adsorption coefficient of 2.6 and an isotopic fractionation factor (a) of 0.975 (Palmer et al., 1987). Fluid composition is that of "Icelandic geothermal water" given above. See text for model details.
[b] from Myvatn
[c] Average of several high-temperature geothermal systems sampled over multiple years